การสังเคราะห์พอลิอะคริลาไมด์/ไมกาซูเปอร์แอบซอร์เบนต์นาโนคอมพอสิตที่มีความเสถียร
เชิงความร้อนและหน่วงการติดไฟ

นายณัฐวุฒ ลิ้มประยูร

SYNTHESIS OF POLYACRYLAMIDE/MICA SUPERABSORBENT NANOCOMPOSITES WITH THERMAL STABILITY AND FIRE RETARDANCY

Mr. Nattawut Limparyoon

A Thesis Submitted in Partial Fulfillment of the Requirements

for the Degree of Master of Science Program in Petrochemistry and Polymer Science

Faculty of Science

Chulalongkorn University

Academic Year 2009

Thesis Title   SYNTHESIS OF POLYACRYLAMIDE/MICA SUPERABSORBENT NANOCOMPOSITES WITH THERMAL STABILITY AND FIRE RETARDANCY

By   Mr. Nattawut Limparyoon

Field of Study   Petrochemistry and Polymer Science

Advisor   Professor Suda Kiatkamjornwong, Ph.D.

Co-Advisor   Nispa Seetapan, Ph.D.

Accepted by the Faculty of Science, Chulalongkorn University in Partial Fulfillment of the Requirements for the Master's Degree

………………………………………Dean of the Faculty of Science

(Professor Supot Hannongbua, Dr.rer.nat.)

THESIS COMMITTEE

………………………………………Chairman

(Professor Pattarapan Prasassarakich, Ph.D.)

………………………………………Thesis Advisor

(Professor Suda Kiatkamjornwong, Ph.D.)

………………………………………Thesis Co-Advisor

(Nispa Seetapan, Ph.D.)

………………………………………Examiner

(Assistant Professor Varawut Tangpasuthadol, Ph.D.)

………………………………………External Examiner

(Wiyong Kangwansupamonkon, Ph.D.)

ฉัฐวุฒ ลิ้มประยูร: การสังเคราะห์พอลิอะคริลาไมด์/ไมกาซูเปอร์แอบซอร์เบนต์นาโนคอม
พอสิตที่มีความเสถียรเชิงความร้อนและหน่วงการติดไฟ (SYNTHESIS OF
POLYACRYLAMIDE/MICA SUPERABSORBENT NANOCOMPOSITES WITH
THERMAL STABILITY AND FIRE RETARDANCY) อ.ที่ปรึกษาวิทยานิพนธ์หลัก:
ศ. ดร. สุดา เกียรติกำจรวงศ์, อ.ที่ปรึกษาวิทยานิพนธ์ร่วม: ดร. นิสภา ศีตะปันย์, 92 หน้า.

ได้สังเคราะห์พอลิ(อะคริลาไมด์-โค-2-อะคริลามิโด-2-เมทิลโพรเพนซัลโซเดียมซัลโฟเนต
เกลือโซเดียม), พอลิ(อะคริลาไมด์-โค-2-อะคริลามิโด-2-เมทิลโพรเพนซัลโซเดียมซัลโฟนิกแอซิด)
และพอลิ(อะคริลาไมด์-โค-2-อะคริลามิโด-2-เมทิลโพรเพนซัลโซเดียมซัลโฟเนต เกลือโซเดียม)/
ซูเปอร์แอบซอร์เบนต์นาโนคอมพอสิตด้วยกระบวนการพอลิเมอไรเซชันแบบเชื่อมขวางด้วยอนุมูล
อิสระ โดยใช้แอมโมเนียมเพอร์ซัลเฟต, เอ็น, เอ็น, เอ็น', เอ็น'-เททระเมทิลเอทิลีนไดแอมีน และ
เอ็น, เอ็น'-เมทิลีนบิสอะคริลาไมด์ เป็นสารริเริ่มปฏิกิริยา, สารริเริ่มปฏิกิริยาร่วม และสารเชื่อม
ขวาง ตามลำดับ การสังเคราะห์ซูเปอร์แอบซอร์เบนต์นาโนคอมพอสิตได้ด้วยการเติมไมกา, ซิงก์
บอเรต และเมลามีน เป็นสารหน่วงไฟ และยังได้ศึกษาอิทธิพลของไอออนิกมอนอเมอร์, สารริเริ่ม
ปฏิกิริยา, สารริเริ่มปฏิกิริยาร่วม, สารเชื่อมขวาง และสารหน่วงไฟ ที่มีผลต่อค่าการดูดซึมน้ำของ
ซูเปอร์แอบซอร์เบนต์นาโนคอมพอสิต ตรวจสอบหมู่ฟังก์ชันหลักของพอลิเมอร์ร่วมด้วยเทคนิค
อินฟราเรดสเปกโทรสโกปี ค่าความเสถียรเชิงความร้อนด้วยการวิเคราะห์น้ำหนักเชิงความร้อน
และโคนคาลอรีเมทรี พบค่าการดูดซึมน้ำเพิ่มขึ้นเมื่อเพิ่มปริมาณของไอออนิกมอนอเมอร์แต่มีค่า
การดูดซึมน้ำลดลงเมื่อเพิ่มสารริเริ่มปฏิกิริยา, สารริเริ่มปฏิกิริยาร่วม, สารเชื่อมขวาง และสารหน่วง
ไฟ มีค่าดูดซึมน้ำสูงสุดที่ 1,212$\pm$54 กรัมต่อกรัม ที่ปริมาณสารริเริ่มปฏิกิริยาและสารริเริ่มปฏิกิริยา
ร่วมอย่างละร้อยละ 0.6 และสารเชื่อมขวางร้อยละ 0.05 ภาวะที่ซูเปอร์แอบซอร์เบนต์นาโนคอมพอ
สิตที่เคลือบบนแผ่นไม้มีค่าความเสถียรเชิงความร้อนสูงสุดด้วยการเติมซิงก์บอเรตร้อยละ 20 โดย
น้ำหนัก และเมลามีนร้อยละ10โดยน้ำหนัก ลงในคอมพอสิต ซึ่งหน่วงการติดไฟได้นานถึง 258
วินาที ก่อนชิ้นไม้ที่เคลือบซูเปอร์แอบซอร์เบนต์นาโนคอมพอสิตจะติดไฟ เมื่อเทียบกับชิ้นไม้ที่
ไม่ได้เคลือบซึ่งติดไฟเพียง 13 วินาที

สาขาวิชา   ปิโตรเคมีและวิทยาศาสตร์พอลิเมอร์   ลายมือชื่อนิสิต..
ปีการศึกษา 2552..   ลายมือชื่อ อ.ที่ปรึกษาวิทยานิพนธ์หลัก..................
ลายมือชื่อ อ.ที่ปรึกษาวิทยานิพนธ์ร่วม..................

5072271023: MAJOR PETROCHEMISTRY AND POLYMER SCIENCE
KEYWORDS: SUPERABSORBENT/MICA   NANOCOMPOSITES/WATER ABSORBENCY/FIRE RETARDANCY

NATTAWUT LIMPARYOON: SYNTHESIS OF POLYACRYLAMIDE/MICA SUPERABSORBENT NANOCOMPOSITES WITH THERMAL STABILITY AND FIRE   RETARDANCY.   THESIS   ADVISOR: PROF.   SUDA KIATKAMJORNWONG, Ph.D.,   THESIS CO-ADVISOR: NISPA SEETAPAN, Ph.D., 92 pp.

Superabsorbent polymers of poly[acrylamide-co-(2-acrylamido-2-methylpropane sulfonic acid sodium salt)], poly(AM-co-AMPS-Na$^+$), poly[acrylamide-co-(2-acrylamido-2-methylpropane sulfonic acid), poly(AM-co-AMPS-H$^+$)] and poly(AM-co-AMPS-Na$^+$) superabsorbent nanocomposites were synthesized by free-radical crosslinking polymerization. Ammonium persulfate (APS), *N, N, N', N'*-tetramethylethylenediamine (TEMED), and *N, N'*-methylenebisacrylamide (MBA) were used as an initiator, a co-initiator, and a crosslinker, respectively. The superabsorbent nanocomposites were produced by adding mica, zinc borate or melamine as fire retardant agents. The influences of ionic comonomer (both the sodium and acid forms) and crosslinker concentrations on the water absorbency of the prepared superabsorbents were investigated. The presence of main function groups of the synthesized copolymers was analyzed using FTIR technique. The thermal stability of superabsorbent nanocomposites was detected by TGA and cone calorimetric technique. The equilibrium water absorbency of poly(AM-co-AMPS-Na$^+$) and poly(AM-co-AMPS-H$^+$) was found to increase with the increase in ionic comonomer concentration, and decrease with the increase in the crosslinker and fire retardant agent loadings. The maximum water absorbency of 1212±54 g g^{-1} was obtained for poly(AM-co-AMPS-Na$^+$) at 85% mol of AMPS-Na$^+$, 0.6% mol each of APS and TEMED, and 0.05% mol of MBA. The superabsorbent nanocomposite/20% zinc borate/10% melamine coated on a wood board increased the ignition time to 258 s from only 13 s ignition time of the uncoated wood.

Field of Study: Petrochemistry and Polymer Science   Student's signature ....

Academic Year: 2009 ....   Advisor's signature ....

Co-Advisor's signature ....

ACKNOWLEDGEMENTS

CONTENTS

LIST OF TABLES

LIST OF FIGURES

| **Figure** | **Page** |

Figure **Page**

LIST OF SCHEMES

LIST OF ABBREVIATIONS

AMPS-H$^+$	2-acrylamido-2-methylpropane sulfonic acid
AMPS-Na$^+$	2-acrylamido-2-methylpropane sulfonic acid sodium salt
AM	acrylamide
APS	ammonium persulfate
N-MBA	*N, N'*-methylenebisacrylamide
TEMED	*N, N, N', N'*-tetramethylethylenediamine
poly(AM-*co*-AMPS-H$^+$)	poly[(acrylamide)-*co*-(2-acrylamido-2-methyl propane sulfonic acid)]
poly(AM-*co*-AMPS-Na$^+$)	poly[(acrylamide)-*co*-(2-acrylamido-2-methyl propane sulfonic acid sodium salt)]
SAPCs	superabsorbent polymer composites
MW	molecular weight
g	gram
g mol^{-1}	gram per mole
g g^{-1}	gram per gram
rpm	revolutions per minute
min	minute
h	hour
ml	milliliter
mg	milligram
mm	millimeter
μm	micrometer

nm	nanometer
Å	Angstrom
° C	degree Celsius
°C min^{-1}	degree Celsius per minute
psi	pound per square inch
% w/w	percentage weight by weight
FTIR	Fourier Transform Infrared Spectrophotometry
XRD	X-ray Diffraction
TEM	Transmission Electron Microscopy
TGA	Thermal Gravimetric Analysis
DTG	Differential Thermal Gravimetry
kV	kilovolt
mA	milliampere
2θ	2-theta

CHAPTER I

INTRODUCTION

1.1 Scientific rational

Superabsorbent polymers (SAPs) are crosslinked hydrophilic polymer networks that can absorb and retain water or biological fluids up to thousands times their dry weight. The presence of crosslinking network prevents the SAPs from the dissolution in medium. Their ability to absorb water is due to the presence of hydrophilic groups such as –CONH, -CONH$_2$, etc. Besides its hydrophilic nature, SAPs containing ionic moiety, or the so-called polyelectrolyte hydrogels, have promoted water absorbency over nonionic hydrogels (Kiatkamjornwong *et al.,* 2000). Several ionic vinyl monomers, such as sodium methacrylate, are used to copolymerize with acrylamide to give high water absorbency SAPs (Kiatkamjornwong *et al.,* 2000). Moreover, 2-acrylamido-2-methylpropane sulfonic acid sodium salt (AMPS-Na$^+$) has been used to copolymerize with acrylamide to give the interesting SAPs because there are adequate numbers of ionizable groups of AMPS-Na$^+$ (Durmaz and Okay, 2000). The product thus has a swelling characteristic whose water absorbency depends on the extent of hydrophilicity and ionizablility of the AMPS-Na$^+$ group.

From its remarkable water absorbency and retention, poly(AM-*co*-AMPS-Na$^+$) superabsorbents are widely used in a wide range of applications, such as support carriers in biomedical engineering, agricultural and fire-retarding applications. Generally, water is used to extinguish fire but most water is evaporated when it contacts fire surface, fire breaking efficiency of water is reduced and wasted. SAPs are used to retard fire spreading. The mechanism of preventing the fire spreading is to cool the surface of the object and to reduce the quantity of oxygen from the surface of the burnable object to a degree such that the flame is self extinguished (Pascente and

Pascente, 1998). However, SAPs cannot endure fire because it is an organic compound which is burnable. Some specific inorganic materials, such as clay and other flame retardants are added in the system for improving SAP thermal stability.

Clay has been used as an inorganic filler to improve physical properties such as modulus, strength, dimension stability, etc (Tjong, 2006). Among various types of clay, mica has been proven to provide the polyacrylamide-SAP composite with the most thermal stability (Zhang and Wang, 2007). Mica has a 2:1 phyllosilicate structure consisting of one octrahedral sheet and two tetrahedral sheets. In this research, mica is used as nanofiller to improve swollen gel strength and thermal properties of superabsorbent polymers for use as a fire retardant material.

Flame retardants are designed for application over a range of combustible and they offer improved aesthetics (Senkowski, 1995). Zinc borate ($2ZnO_2B_2O_3.3H_2O$) is an effective inorganic flame retardant and it possesses characteristic properties of flame retardancy, smoke suppression, promoting charring, etc. (Nazare *et al.*, 2008) particularly important according to new fire standards. Zinc borate is commonly used as a multifunction flame retardant in combination with other halogenated or halogenated free flame retardant systems to boost flame retardancy properties (Wu and Yang, 2007). Melamine and its derivatives are especially useful for suppressing smoldering because it can generate N_2 to dilute O_2 gas.

1.2 Objectives of the research work

The objectives of this research are as follows:

1.2.1   To synthesize SAPs of acrylamide copolymers with 2-acrylamido-2-methylpropane sulfonic acid and its sodium salt in order to investigate the suitably ionic comonomer (either salt or acid) to produce SAPs with better swelling performance in water.

1.2.2   To synthesize the superabsorbent of poly[(acrylamide)-*co*-(2-acrylamido-2-methyl propane sulfonic acid sodium salt)] by solution polymerization. Effects of reaction parameters such as monomer ratio, initiator, co-initiator, and crosslinking content on equilibrium water absorbency were investigated.

1.2.3   To synthesize the superabsorbent of poly[(acrylamide)-*co*-(2-acrylamido-2- methyl propane sulfonic acid sodium salt)]/mica nanocomposites by solution polymerization. Effects of mica content on equilibrium water absorbency in deionized water and tap water and on thermal stability of SAP composites were investigated.

1.2.4   To synthesize the superabsorbent of poly[(acrylamide)-*co*-(2-acrylamido-2- methyl propane sulfonic acid sodium salt)]/fire retardant (i.e., zinc borate and melamine) by solution polymerization. Effects of fire retardant content on equilibrium water absorbency in deionized water and tap water and on thermal stability of SAPs composites were investigated. In this study, individual fire retardant and the mixture of zinc borate and melamine at various ratios of loading were investigated.

1.3 Expected outcome obtainable from the research

1.3.1 To obtain the poly[(acrylamide)-*co*-(2-acrylamido-2-methylpropane sulfonic acid sodium salt)] that absorb sufficient amounts of water suitable for use as a guideline for the following synthesis of superabsorbent nanocomposites with improved thermal stability.

1.3.2 To achieve the SAPs composites with mica, zinc borate, melamine, and mixed zinc borate and melamine having adequate water absorption, thermal stability and improved fire retardancy properties.

1.4 Scope and work plan

Superabsorbents of acrylamide copolymers with ionic monomers (i.e., 2-acrylamido-2-methylpropane sulfonic acid and its sodium salt) were synthesized at various AM-to-ionic monomer ratios from 98:2 to 15:85. The polymerization was carried out at 60 ^{o}C for 30 min at fixed contents of N-MBA, APS and TEMED used as a crosslinking agent, an initiator and co-initiator, respectively. The form of ionic monomer providing the highest amount of water absorbency was selected for further investigations. The suitable contents of N-MBA, APS, TEMED, and the quantity of water present in the polymerization reaction were investigated and selected to prepare SAP nanocomposites. The work plan is therefore set as follows:

1.4.1 Synthesis of SAPs by varying the ionic comonomer ratios for the highest water absorbency

1.4.2 Synthesis of SAPs through the solution polymerization by varying the following parameters:

1.4.2.1 The effect of *N, N'*-methylenebisacrylamide (N-MBA) content at 0.05, 0.10 and 0.2% mol of the total monomer on the equilibrium water absorbency.

1.4.2.2 The effect of deionized water amount in the reaction at 10 and 20 ml on the equilibrium water absorbency.

1.4.2.3 The effect of *N, N, N', N'*-tetramethylethylenediamine (TEMED) content at 0.6, 1.2 and 1.8% mol of total monomer on equilibrium water absorbency.

1.4.2.4 The effect of ammonium persulfate (APS) content at 0.6, 1.2 and 1.8% mol of total monomer on equilibrium water absorbency.

1.4.3 Synthesis of SAP/mica nanocomposites via intercalative polymerization by varying the following parameters:

1.4.3.1 Synthesis of modified mica and SAP/modified mica nanocomposites by varying modified mica contents on d-spacing and equilibrium water absorbency.

1.4.3.2 The effect pure mica content at 5, 10, 20 and 30% w w^{-1} of total monomer on equilibrium water absorbency in deionized water and tap water.

1.4.4 Synthesis of SAP/zinc borate nanocomposites by varying the following parameters: The effect of zinc borate content at 5, 10, 20 and 30% w w^{-1} of total monomer on equilibrium water absorbency in deionized water and tap water.

1.4.5 Synthesis of SAP/melamine nanocomposites by varying the following parameters: The effect of melamine content at 5, 10, 20 and 30% w w^{-1} of total monomer on equilibrium water absorbency in deionized water and tap water.

1.4.6 Synthesis of SAP/zinc borate/melamine nanocomposites by varying the following parameters: The effect of zinc borate-to-melamine ratios at 30:0, 20:10, 15:15, 10:20 and 0:30% w w^{-1} of total monomer on equilibrium water absorbency.

1.4.7   Characterization of the synthetic products

1.4.7.1 Identification of functional groups of poly(AM-*co*-AMPS-H$^+$) superabsorbent, poly(AM-*co*-AMPS-Na$^+$) superabsorbent, SAPs nanocomposites with the addition of mica, zinc borate, melamine, and the mixture of zinc borate and melamine.

1.4.7.2 Investigation of water absorbency of the SAPs and the SAP nanocomposites.

1.4.7.3 Investigation of the intercalation morphology of poly(AM-*co*-AMPS-Na$^+$)/mica nanocomposite by transmission electron microscopy.

1.4.7.4 Characterization of poly(AM-*co*-AMPS-Na$^+$)/mica nanocomposite by X-ray diffraction.

1.4.7.5 Thermal properties of the SAPs and SAP nanocomposites by thermal gravimetric analysis.

1.4.7.6 Flame retardancy properties of the poly(AM-*co*-AMPS-Na$^+$)/zinc borate/melamine superabsorbent nanocomposite by cone calorimetry.

CHAPTER II

THEORY AND LITERATURE REVIEW

2.1 Superabsorbent polymers

Superabsorbent polymers (SAPs) are three-dimensional crosslinked hydrophilic, linear or branched polymers with the ability to absorb large quantities of water, saline or physiological solutions compared with general absorbing materials (Pourjavadi *et al*., 2004). Because of their excellent hydrophilic properties, high swelling ratio, and biocompatibility, hydrogels have been widely used in agriculture (Ibrahim *et al*., 2007), biomedical area as antibacterial materials (Murthy, 2008), tissue engineering (Kim, 2008), biosensors (Adhikari and Majumdar, 2004), sorbents for the removal of heavy metals (Guilherme *et al*., 2007), and drug delivery (Rodriguez *et al*., 2003). Usually, most hydrogels were prepared from synthetic polymers by radical copolymerization (Yue *et al.*, 2009), frontal copolymerization (Yan *et al*., 2005), graft copolymerization (Zhang *et al.*, 2006), cross-linking (Marandi *et al*., 2008), and ionizing radiation (El-Rehim *et al*., 2006).

2.1.1 Mechanism of swelling of superabsorbent polymers

The polymer backbone in SAPs is hydrophilic because it contains water-solubilizing groups, such as $-OH$, $-COOH$, $-CONH_2$, $-CONH-$, $-SO_3H$, and so on. SAPs therefore can be neutral or ionic in nature. The insolubility of the hydrophilic SAPs is caused by the presence of a three dimensional network. When water is added to SAPs, there is a polymer-solvent interaction via hydration and the formation of hydrogen bonds (Elliot, 2004).

2.1.1.1 Hydration

Hydration is the interaction of ions of a solute with molecules of a solvent, for instant, COO^- and Na^+ ions attract the polar water molecules (Figure 2.1).
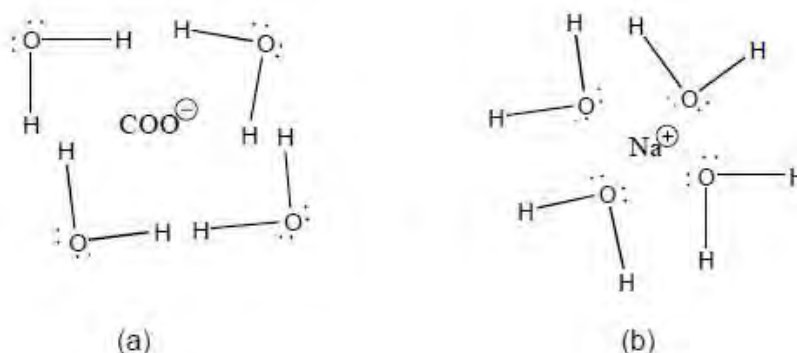
Figure 2.1 (a) COO^- and (b) Na^+ ions attract the polar water molecules (Elliot, 2004)

2.1.1.2 Hydrogen Bond

Hydrogen bond is an electrostatic interaction between molecules containing hydrogen atoms attached to small electronegative atoms such as N, F and O. Hydrogen atoms are attracted to the non-bonding electron pairs (lone pairs) on other neighboring electronegative atoms (Figure 2.2).

In water, the electronegative atom is oxygen which pulls electrons of hydrogen towards itself setting up a dipole in the molecule. The positive hydrogen atoms are attracted to the oxygen lone pairs on other water molecules. Oxygen has two lone pairs of electrons and each is capable of hydrogen bonding to other two water molecules (Elliot, 2004).
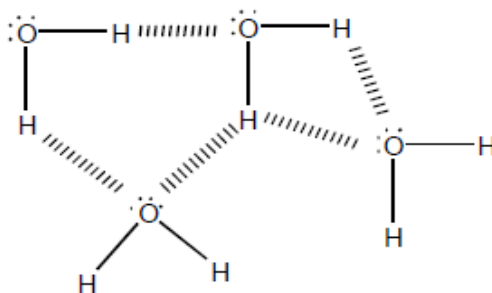
Figure 2.2 Hydrogen bond of water could attract near other molecules

The expansion of hydrogel in water increases due to the absorbed water. The presence of the crosslinked polymer chains resists the swelling of hydrogel by elastic retraction forces of the polymeric network. The lower degree of crosslinking reaction leads to a higher degree of swelling due to a higher expansion of polymer chains (Garcia-González *et al.,* 1993; Pourjavadi *et al.,* 2004). The more polymer chains separate from each other, the more stiffness the coiled polymer chains become. Finally, it reaches equilibrium of swelling by a balance between the infinite dilution of the chains and the retraction forces.

For ionic hydrogel, there is a polymer-solvent interaction including a more simple mixing term. In Figure 2.3, the hydrogel bears electrical charges along the polymer chains (Buchholz and Burgert, 1996). The negative charges of the carboxylate groups in hydrogel repulse one another and are compensated with the positive charges of sodium ions to maintain electrical neutrality. When the hydrogel is added in water, water molecules diffuse into the network of hydrogel and solvate sodium ions. The attractive forces between the negative charges of carboxylate groups and sodium ions are lower due to a high dielectric constant of water. In salt solutions, sodium ions are freely moveable within

the hydrogel network but they cannot leave the gel because of the weak attraction forces with the negative carboxylate ions. Thus, they are trapped in hydrogel as these in a semi-permeable membrane. The difference between the osmotic pressure inside and outside the hydrogel is the driving force for swelling. When the salinity outside the hydrogel increases, the osmotic pressure is lowered and reduces the swelling capacity of hydrogel. The maximum swelling of hydrogel occurs in deionized water (Buchholz and Burgert, 1996).
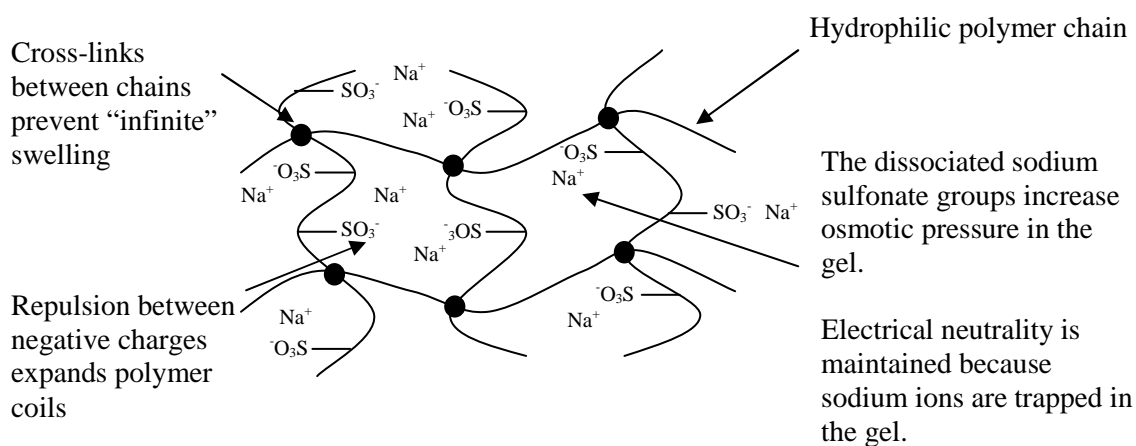
Figure 2.3 Mechanism of swelling of ionic hydrogel adapted form (Buchholz and Burgert, 1996)

2.1.2 Factors affecting the swelling of ionic superabsorbent

2.1.2.1 Effect of ionic content

With the increase of ionic monomer ratio, the number of ionizable groups in the hydrogel increases. This consequently causes an increase of water absorbency. In addition, the more hydrophilicity of the hydrogel enhanced by the ionic monomer causes a stronger affinity for absorption of water (Fatang *et al*., 2006). In this case, increasing degree of equilibrium swelling with increasing ionic

group contents of the hydrogels is expected. This is a consequence of the osmotic pressure exerted by counter ions of the ionic units in the network chains. This osmotic pressure increases as the concentration difference of the counter ions between the inside and outside the gel phase increases (Durmaz and Okay, 2000).

2.1.2.2 Effect of crosslink density

The crosslink density is often defined as the mole fraction of monomer units that are crosslinked. Crosslinking provides anchoring points for the polymer chains and these points restrain excessive movement and maintain the position of the chain in the network. Thus, when a higher concentration of crosslinker is employed, the number of crosslink points in the polymer network increases, resulting in a denser and more compact hydrogel structure. Therefore, rate of diffusion of water molecules into the hydrogel decreases. This is because a hydrogel with a higher crosslink density shows more resistance to matrix expansion, therefore, less water is absorbed slowly. Consequently, water diffuses less readily inside the dense hydrogel structure since the interactions between the water molecules and the ionizable groups are more restricted which is supported by the observation that the lower crosslink density gives softer and less elastic hydrogel (Nalampang *et al*., 2007).

2.1.2.3 Effect of salt solution

For the ionic hydrogel, the ions attached to the polymer network in the hydrogel are immobile and are considered to be separated from the external solution by a semi-permeable membrane, which confines to the immobile ions, but gives passage to water an all simple ions. When the hydrogels are immersed in the external medium, the mobile ions from the external solutions have diffused through the membrane to the interior of gels to maintain electrical neutrality on the

both sizes of the membrane. The amount of mobile ions diffused from external solution to the interior of gel is inversely proportional to the concentration of non-diffusible ion within the polyelectrolyte hydrogel. The decreased swelling ratio of the hydrogels with increasing salt concentration in the external solution is therefore expected due to a decrease in the concentration difference of counter ions inside and outside the hydrogels (Okay and Sariisik, 2000).

2.2   Clay-polymer nanocomposites

Clay is a very fine grained, unconsolidated rock matter, which is plastic when wet, but becomes hard and stony when heated. It has its origin in natural processes, mostly complex weathering, transported and deposited by sedimentation within geological periods. Clay is composed of silica (SiO_2), alumina (Al_2O_3) and water (H_2O) with appreciable concentrations of oxides of iron, alkali and alkaline earth, and contains groups of crystalline substances known as clay minerals such as quartz, feldspar, and mica. Clay is an additive such as sawdust and ashes on the thermal conductivity of clay with no moisture content. Clay with low thermal conductivity can serve many purposes such as a clay oven for baking and drying, a good insulator between two metal surfaces where heat is to be conserved within a certain area and heat loss by conduction is to be prevented (Folaranmi, 2009).

The clay structure is a combination of tetrahedral and octahedral sheets. A tetrahedral sheet occurs by a silica atom coordinated with other elements, whereas an octahedral sheet composes of Al^{3+}, Mg^{2+} or/and Fe^{2+}. The ratios of the tetrahedral to the octahedral sheets in clay mineral are 1: 1 or 2: 1 phyllosilicates (Tjong, 2006).

Kaolinite clay is a 1:1 phyllosilicate, composed of one layer each of tetrahedral and one octahedral structure as shown in Figure 2.4. Its formula is

$Al_2(Si_2O_5)(OH)_4$. Both octahedral and tetrahedral sheets do not have any charges. Thus, neither anions nor cations can occupy the space between the silicate layers. Hydrogen bonding between oxygen atom in the tetrahedral sheets and hydroxyl groups in the octahedral sheets of the adjacent layers are the forces that hold together silicate layers (Zeng *et al.,* 2005).
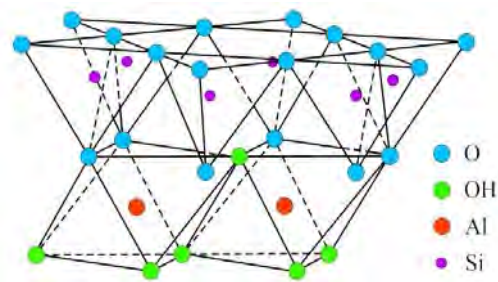
Figure 2.4 Structure of a 1:1 phyllosilicate

Mica is known as a 2: 1 phyllosilicate as shown in Figure 2.5 (Ray and Okamoto, 2003). The crystal lattice of a 2: 1 phyllosilicate consisting of two-dimensional layers of an edge-shared octahedral sheet is fused to two tetrahedrals by the shared oxygen ions of one octahedral sheet and two tetrahedral sheets (Tjong, 2006). Thus, mica has positively charged ions between the layers. It is known as the interlayer cations (A). The general formula of mica is $AM_{2\text{-}3}T_4O_{10}X_2$, where A is usually Na, K or Ca; M is Fe, Al and Mg; T is Si and/or Al; and X is (OH), O, Cl and F (Bozhilov *et al.*, 2008).
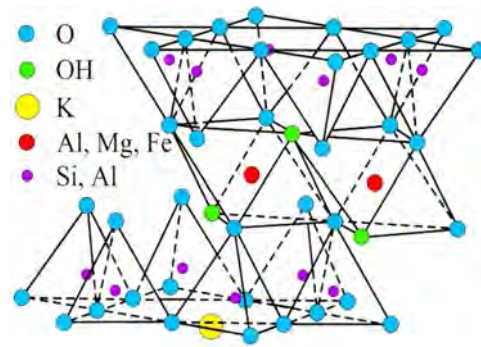
Figure 2.5 Structure of a 2:1 phyllosilicate (Tjong, 2006)

Types of nanocomposites

Nanocomposites containing a polymer and clay mineral, such as mica, can exhibit three types of polymer layered silicate structure as shown in Figure 2.6 (Tjong, 2006). Each type depends on the strength of interfacial interactions between silicate layers and the polymeric matrix in nanocomposites.

a) Flocculated structure   b) Intercalated structure   c) Exfoliated structure
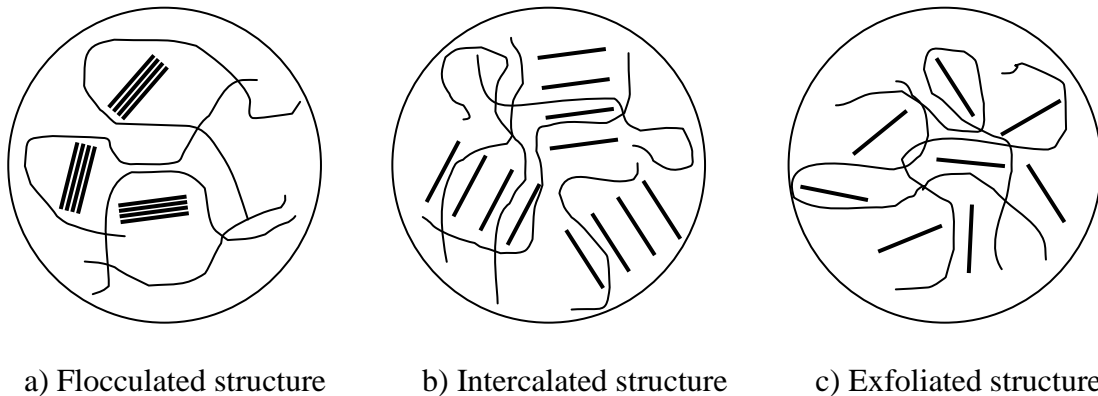
Figure 2.6 Three different types of polymer layered silicate nanocomposites

As illustrated in Figure 2.6a, the space of silicate layers in flocculated nanocomposite is smaller than that of the intercalated nanocomposite. The flocculation or intercalation of the silicate layers results in by the interaction between the edges of each silicate layer. On the other hands, the space between silicate layers

in intercalated nanocomposite (Figure 2.6b) is expanded due to the insertion of polymer chains into the layered silicate structure. This results in the well-ordered multilayer morphology in nanocomposites with a few nanometers repeating distance. In case of the exfoliated nanocomposite (Figure 2.6c), the individual silicate layers of clay are separated by the inserted polymer chains. When the lower content of clay is used, the higher tendency to form exfoliated nanocomposite becomes.

2.3   Organo-clay modification

Quaternary ammonium cations, also known as quats, are positively charged polyatomic ions of the structure NR_4^+ with R being alkyl groups. Unlike the ammonium ion (NH_4^+) and the primary, secondary, or tertiary ammonium cations, the quaternary ammonium cations are permanently charged, independent of the pH of their environment.

Most methods have dealt with exchanging cations in the clay galleries with long-chain aliphatic quaternary ammonium or phosphonium compounds. This substitution increases clay gallery spacing and creates a more favorable organophilic environment for polymer penetration and interaction (He and Zhang, 2006). Modified clay is frequently used in the scientific research. Ion exchange of the sodium ions in the gallery of the clays with the polymeric quaternary ammonium ions is the most favorable method used in industries because of its lower cost (Chen *et al*., 2007).

2.4   Fire retardant

Several commercial polymers are flammable, causing the loss of life and possessions. Therefore, it is mandatory to improve their fire retardancy to meet the fire safety requirements. To achieve such a property, the addition of a flame retardant

during synthesis or processing of the polymers has been increasingly used to reduce combustibility and to suppress smoke or toxic gas released from the flaming polymers. Research and development, and the industrial production of flame retardants have been developed during the past decades which can be classified as follows (Innes, 1996).

2.4.1 Halogen-containing flame retardants

It is well-known that all kinds of flame retardants act either in the vapor phase, the condensed phase or both phases through a chemical and/or physical mechanism to interfere with the combustion process during heating, pyrolysis, ignition, or flame spread (Li *et al*., 2003). Particularly, halogenated compounds act mostly in the vapor phase by a radical mechanism to interrupt the exothermic processes to suppress combustion.

2.4.2 Inorganic flame retardants

Metal hydroxides can be used as flame retardants in polymer materials due to their low toxicity, anti-corrosion properties, low cost, and low emission of smoke during processing and burning. Among metal hydroxides, magnesium hydroxide, $Mg(OH)_2$, and aluminum hydroxide, $Al(OH)_3$ are the two most important classes. Generally, the flame-retardant mechanism of metal hydroxides is endothermic decomposition into the respective oxides and water when heated, and the released water vapor isolates the flame and dilutes the flammable gases in the gas phase. However, they have some serious disadvantages such as low flame-retardant efficiency and thermal stability, and great deterioration in the physical and mechanical properties of the matrices (Chen and Wang, 2009)**.**

2.4.3   Organic phosphorus/nitrogen flame retardants

The organic flame retardants which contain phosphorus or nitrogen species have attracted much attention. Some researchers (Lui *et al.*, 2009; Schartel *et al.*, 2006) have done many significant works for improving the flame retardant properties of polymers using these flame retardants. The range of phosphorus-containing flame retardants is extremely wide since the element exists abundantly. Phosphines, phosphine oxides, phosphonium compounds, phosphonates, phosphites, and phosphate are examples for this type of flame retardants used in polymers (Ou and Li, 2006).

2.4.4   Inherent flame-retardant systems

Inherent flame-retardant polymers are the systems that are not physically added into the polymer matrices, but the flame-retardant elements or groups are chemically bonded into the molecular chains of the original polymers (Wang, 1997). For examples, flame retardant polyurethanes containing phosphorus that can react with isocyanate have been synthesized. Wang *et al.* (2001) prepared the flame retardant polyurethane foam (PUF) with diethyl N,N′-diethanolamino-methylphosphate and isocyanate. The flame retardant PUFs have high flame retardant properties, and the limiting oxygen index (LOI) value is 29. Ma *et al.* (1997) synthesized phosphorus-containing polyurethanes by a novel reaction of phosphorus-containing diisocyanates and diols. The phosphorus containing polyurethanes have high flame retardant properties; the LOI values of these polyurethanes are around 29–33. Inherent flame-retardant polymers have received increasing interest in academic and industrial applications (Chen and Wang, 2009).

2.5   Literature survey

This section briefly describes the general aspects and cross-linking polymerization of superabsorbent polymers (SAPs) and superabsorbent polymer composites (SAPCs). Research and development of SAPs has become very active after the Northern Region Laboratory of the United States Department of Agriculture invented the first SAP, used as a soil conditioner. Based on the advancements in organic/inorganic syntheses, SAPs are produced and used in a wide range of applications for fluid absorption. The rapid growing nanotechnology has led to more explorations of SAPs and SAPCs for applications in biomedical, biotechnology and advanced technologies. Examples of research work of SAPs and SAPCs published in refereed, reviewed articles are introduced (Kiatkamjornwong, 2007).

Durmaz and Okay (2000) synthesized acrylamide (AAm)/2-acrylamido-2-methylpropane sulfonic acid sodium salt (AMPS)-based hydrogels and investigated their swelling behavior. The hydrogels were prepared by free-radical crosslinking copolymerization of AAm and AMPS at 40°C in the presence of N,N'-methylene-bisacrylamide (BAAm) as the crosslinker. The AMPS content in the monomer mixture was varied from 0 to 100% mol. It was found that the copolymer composition is equal to the monomer feed composition, indicating that the monomer units distribute randomly along the network chains of the hydrogels. The equilibrium degree of swelling of the prepared hydrogels increases with increasing AMPS content until a plateau is reached at about 10% mol AMPS. Between 10 and 30% mol AMPS, the equilibrium gel swelling in water as well as in aqueous NaCl solutions was independent on the ionic group content of the hydrogels. Further increase in the AMPS content beyond this value increased the gel swelling continuously up to 100% mol where the maximum water absorbency of about 1600 g g^{-1} was obtained.

Naghash and Okay (1996) synthesized acrylamide/N,N'-methylenebis acrylamide (Bis) copolymeric hydrogels. Conversion of monomer and pendant vinyl groups was measured as a function of the reaction time up to the onset of macrogelation. Experimental results indicated that 80% mol of pendant vinyl groups were consumed by cyclization reactions. The equilibrium degree of swelling of the polyacrylamide (PAAm) gels was independent of their crosslinker content. Calculation results showed that the average reactivity of pendant vinyl groups for intermolecular links decreased as the Bis concentration increased. All these results suggest a formation of PAAm microgels prior to the onset of macrogelation. As the reaction proceeds, microgels are connected to a macrogel through their peripheral pendant vinyls and radical ends, whereas those in their interior remain intact. The microgels seem to act as the junction points of the final inhomogeneous networks.

Bordado and Gomes (2007) pointed out that fire extinction with water could be significantly improved by adding SAPs into the water used to extinguish fire, or spraying swelling SAPs over surfaces of combustible objects in order to protect them from fire spreading. They focused on the newly developed poly(acrylamide-co-2-acrylamide-2-methyl-propane-sulphonate) SAPs and proposed that this SAP seemed to have particularly efficient for fire-fighting purpose in terms of its high water absorption.

Zhang and Wang (2007) investigated the type and quantity of clays on reaction mechanism, thermal stability, equilibrium water absorbency, swelling rate, and other swelling properties of clay-based acrylamide superabsorbent composites. Various types of clays understudy were attapulgite, kaolinite, mica, vermiculate and Na^+-montmorillonite. The superabsorbent composites were prepared by free-radical aqueous polymerization, using N,N'-methylenebisacrylamide as a crosslinker and

ammonium persulfate as an initiator, and then saponified with sodium hydroxide solution. The FTIR, XRD and TGA were employed to characterize the prepared composites. The results indicated that mica improved thermal stability of corresponding superabsorbent composites to the highest degree comparing with the other clays. All PAM/clay superabsorbent composites incorporated with 10% w w^{-1} of clay provided the equilibrium water absorbency of more than 1300 g g^{-1}. The equilibrium water absorbency decreases with increasing clay content and correlates with the type of clays. Attapulgite-based superabsorbent composite had higher water absorbency in univalent cationic saline solution, however, the vermiculite- and the kaolinite-based SAPs acquired the highest water absorbency in $CaCl_2$ and $FeCl_3$ aqueous solution, respectively. Moreover, the superabsorbent composites incorporated with Na^+-montmorillonite had higher swelling rate and that doped with mica was endowed with higher reswelling capability.

Zhang *et al*. (2007) synthesized a chitosan-*g*-poly(acrylic acid)/attapulgite superabsorbent composite with water absorbency of 160 g g^{-1} in distilled water and 42 g g^{-1} in 0.9% w w^{-1} of NaCl solution. N,N′-methylenebisacrylamide was used as a crosslinker while ammonium persulfate was employed as an initiator. The result from FTIR spectra showed that –OH of attapulgite, –OH, –NHCO and –NH$_2$ of chitosan participated in graft polymerization with acrylic acid. The introduced attapulgite enhanced thermal stability of the chitosan-*g*-poly(acrylic acid) superabsorbent and formed a loose and more porous surface. Introducing a small amount of attapulgite also enhanced water absorbency of the chitosan-*g*-poly(acrylic acid) superabsorbent.

Weian *et al.* (2005) synthesized hydrogel nanocomposites of a novel organophillic montmorillite (OMMT). The OMMT was also used as a crosslinking agent as well because its intercalating agent contains two double bonds (C=C).

OMMT was prepared through cationic exchange between Na+-montmorillonite and the 2-methacryloyloxyethyl allyldimethylammonium bromide (an intercalating agent) in an aqueous solution. The sheets of the OMMT clay are well-dispersed in this nanocomposite as an exfoliated structure as confirmed by XRD. The hydrogel nanocomposites have higher thermal properties and swelling ratio than the conventional hydrogel.

Lu *et al.* (2008) prepared ethylene-octene copolymer (POE)-based nanocomposites from POE or maleic anhydride grafted POE with organo-modified montmorillonite (OMT) using a melt blending technique. Their morphology, flammability, and crystallization behavior were investigated by X-ray diffraction (XRD) and transmission electron microscopy (TEM), cone calorimeter, and differential scanning calorimetry (DSC), respectively. The XRD and TEM studies confirmed the intercalation of clay layers within the POE matrix whereas the exfoliation was found throughout the maleated POE matrix. Cone calorimetry results exhibited that the reduction in heat release rate of exfoliated maleated-POE/OMT nanocomposite was greater than that of intercalated POE/OMT nanocomposite. The DSC data suggested that the nonisothermal kinetics crystallization of the exfoliated nanocomposite corresponded to tridimensional growth with heterogeneous nucleation.

Braun *et al.* (2007) investigated the fire retardancy mechanisms of aluminium diethylphosphinate in combination with melamine polyphosphate and zinc borate in glass-fiber reinforced polyamide 6,6. The influence of phosphorus compounds on the polyamide decomposition pathways was characterized using thermal analysis (TG), evolved gas analysis (TG-FTIR), and FTIR-ATR analysis of the residue. The Lewis acid-base interactions between the flame retardants, the amide unit, and the metal ions controlled the decomposition. The flammability (LOI, UL 94) and performance under

forced-flaming conditions (cone calorimeter using different irradiations) were investigated. Fire residues were analyzed with FTIR, ATR, SEM, EDX, and NMR. Aluminium phosphinate in polyamide 6,6 acts mainly by flame inhibition. Melamine polyphosphate shows some fuel dilution and a significant barrier effect. Using a combination of aluminium phosphinate and melamine polyphosphate results in some charring and a dominant barrier effect. These effects were improved by the presence of zinc borate due to the formation of boron-aluminium phosphates instead of aluminium phosphates.

Koytepe *et al.* (2009) developed the novel polyimide–zinc borate hybrid nanocomposite films (PI/zinc borate) from the poly(amic acid) of 2,6-diaminopyridine with different weight percentages of zinc borate (1-10% w w^{-1}). The microstructures and morphology of the obtained samples were studied by X-ray diffraction, infrared spectra, scanning electron microscopy equipped with an energy-dispersive X-ray spectrometer, transmission electron microscopy and thermogravimetric analysis. The nanocomposites exhibited increased heat resistant properties. The SEM–EDX analysis showed a homogenous dispersion of zinc borate in the polyimide matrix. The thermal stability of the composite films was found to increase with zinc borate loadings.

Cai *et al.* (2008) prepared the halogen-free flame retardant form — stable phase change materials (PCM) based on paraffin/high density polyethylene (HDPE) composites using a twin-screw extruder technique. Expandable graphite (EG) and different synergistic additives, such as ammonium polyphosphate (APP) and zinc borate (ZB) were used as well. The TGA results showed that the halogen-free flame retardant composites produced a larger amount of charred residue at 700°C. The DSC results indicated that the additives of flame retardant had little effect on the thermal energy storage property, and the temperatures of phase change peaks and the latent

heat of the paraffin occurred easily during the freezing process. The dynamic FTIR monitoring results revealed that the breakdowns of main chains (HDPE and paraffin) and formations of various residues increased with increasing thermo-oxidation temperature. It was also found from the calorimetric tests that the peak of heat release rate (PHRR) decreased significantly. Both the decrease of the PHRR and the structure of charred residue after combustion indicated that there was a synergistic effect between the EG and APP, contributing to the improved flammability of the halogen-free flame retardant form ─ stable PCM composites.

CHAPTER III

EXPERIMENTAL

3.1 Chemicals and Materials

3.1.1 Acrylamide (AM), industrial grade from Siam Chemical Industry Co., Ltd. (Bangkok, Thailand), C_3H_5NO, solid, MW = 71.08 g mol^{-1}

3.1.2 2-Acrylamido-2-methylpropane sulfonic acid sodium salt (AMPS-Na$^+$), analytical grade from Aldrich (Steinhiem, Germany), $C_7H_{15}O_4NSNa$, liquid, MW = 207.25 g mol^{-1}

3.1.3 2-Acrylamido-2-methylpropane sulfonic acid (AMPS-H$^+$), analytical grade from Aldrich (Steinhiem, Germany), $C_7H_{16}O_4NS$, liquid, MW = 184.12 g mol^{-1}

3.1.4 Swelling mica, industrial grade from Wako Pure Chemical Industries (Osaka, Japan), $K_2Al_4(Al_2Si_6O_{20})(OH)_4$, solid, average particle size = 3 μm

3.1.5 2-(dimethylamino)ethyl methacrylate, analytical grade from Aldrich (Steinhiem, Germany), $C_8H_{15}O_2N$, liquid, MW = 157.21 g mol^{-1}

3.1.6 Allyl bromide, analytical grade from Aldrich (Steinhiem, Germany) C_3H_5Br, liquid, MW = 120.98 g mol^{-1}

3.1.7 Hydroquinone mono methyl ether (HMQE), analytical grade from Aldrich (Steinhiem, Germany), $C_7H_8O_2$, liquid, MW = 124.14 g mol^{-1}

3.1.8 Zinc borate (Zb), analytical grade from Aldrich (Steinhiem, Germany) ZnB_4O_7, solid, MW = 220.61 g mol^{-1}

3.1.9 Melamine (Mm); industrial grade from Siam Thai Mitsui Specialty Chemicals Co., Ltd. (Chachoengsao, Thailand), $C_3H_6N_6$, solid, MW = 126.12 g mol^{-1}

3.1.10 *N,N′*-Methylenebisacrylamide (N-MBA), analytical grade from Fluka (Buchs, Switzerland), $C_7H_{10}N_2O_2$, solid, MW = 154.17 g mol^{-1}

3.1.11 Ammonium persulphate (APS), analytical grade from Ajax (Seven Hills, Australia), $(NH_4)_2S_2O_8$, solid, MW = 228.20 g mol^{-1}

3.1.12 *N,N,N',N',*-Tetramethylethylenediamine (TEMED), analytical grade from Fluka (Buchs, Switzerland), $C_6H_{16}N_2$, liquid, MW = 116.21 g mol^{-1}

3.1.13 Acetone, from BDH (Bangkok, Thailand) $C_3H_6O_2$, liquid, MW = 58.08 g mol^{-1}

3.1.14 Potassium bromide, analytical grade from Ajax (Seven Hills, Australia) KBr, solid, MW = 119.01 g mol^{-1}

3.1.15 Wood board made from Apocynaceae, Wrightia religiosa *Benth*.

3.2 Glassware

3.2.1   1000-ml four-necked glass reactor

3.2.2   Liebig condenser

3.2.3   Alcohol-in-glass thermometer

3.2.4   Volumetric flask

3.2.5   Pipette

3.2.6   Beaker

3.2.7   Soxhlet apparatus

3.2.8   Other general laboratory glassware

3.3 Equipment

3.3.1   Stirring type: A half-moon shaped Teflon blade agitator

3.3.2   Mechanical stirrer: IKA Werke GmbH & Co. KG, Staufen, Germany

3.3.3   Flow meter: Omega, Tokyo, Japan

3.3.4   Water purifier: Elga Lab water LA 611, Veolia Systems Ltd, Buckinghamshire, UK.

3.3.5   Water bath: Memmert W 350, Memmert GmbH & Co. KG, Swabach, Germany

3.3.6   Analytical balance: Metter AE 260, Mettler-Toledo, Inc., Greifensec, Switzerland

3.3.7   Oven: D 7200, Binder GmbH & Co. KG, Tuttlingen, Germany

3.3.8   Magnetic stirrer: Yamamoto Mag-mixer MD-200, Yamamoto Scientific Co. Ltd, Tokyo, Japan

3.3.9   Fourier Transform Infrared Spectrometer (FTIR): Perkin Elmer, Spectrum GX, Massachusetts, USA

3.3.10 Transmission Electron Microscope (TEM): Jeol model JSM-6400, Tokyo, Japan

3.3.11 X-Ray Diffraction (XRD): DMAX 2200/Ultima, Tokyo, Japan

3.3.12 Thermal Gravimetric Analysis (TGA): TGA/SDTA 851^{e}, Mettler Toledo Corporation, Switzerland.

3.3.13 Cone Calorimeter: Dual Cone Calorimeter Fire Testing Technology Limited, UK

3.4 Procedure

3.4.1   Synthesis of acrylamide copolymeric superabsorbents

AM, ionic monomer (either AMPS-H^{+} or AMPS-Na^{+}), and N-MBA (crosslinker) were dissolved in deionized water in a 1000-ml four-necked glass reactor equipped with a mechanical stirrer assembled with a half moon Teflon blade paddle and the mixture was stirred for 20 min at room temperature. The solution was

heated at 60°C in water bath under nitrogen atmosphere. APS (initiator) was added and stirred for 5 min, and TEMED (co-initiator) was then added. The mixture was stirred at 250 rpm for 30 min. Then the reaction was cool down to room temperature and dewatered with acetone. The product was dried in an oven at 50 $^{\circ}$C for 24 h and subsequently extracted with acetone in a Soxhlet apparatus for 12 h to remove homopolymers. The extracted product was dried in an oven at 50 $^{\circ}$C for 24 h. Finally, the resulting polymer was milled and sieved through a 100-mesh sieve.

3.4.1.1 *Effect of the form of ionic monomer (AMPS-H$^+$ and AMPS-Na$^+$) and the ratio of monomers*

The experimental procedure as described in Section 3.4.1 was carried out with various molar ratios of AM:ionic monomer from 98:2 to 20:80 at a fixed concentration of APS, TEMED, and N-MBA of 1.2%, 1.2%, and 0.2% by mol of the monomers, respectively. In this study, 40 ml of water was also added into the polymerization. The form of ionic monomer (either acid or salt) and the ratio of monomers on equilibrium water absorbency of the synthesized superabsorbents was optimized to prepare SAPs having higher degree of water absorbency.

3.4.1.2 *Effect of the amount of crosslinker and the degree of monomer dilution*

Effect of the amount of crosslinker and the degree of monomer dilution were studied using the same procedure described in Section 3.4.1. The contents of APS and TEMED were set at 1.2 and 1.2% mol of total monomer, respectively. The molar ratio of AM:AMPS-Na+ was fixed at 15:85. Various crosslinker (N-MBA) contents from 0.05 to 0.2 %mol of total monomer and the amount of water at 10 and 40 ml were studied to investigate the role of crosslinker

content and the degree of monomer dilution on water absorbency of the resulting SAPs.

3.4.1.3 Effect of amounts of co-initiator and initiator

The same experimental procedure as described in Section 3.4.1 was carried out with various co-initiator (TEMED) contents from 0.6 to 2.4% mol of total monomer when the N-MBA crosslinker and initiator were fixed at 0.05 and 1.2 %mol of total monomer, respectively, and the mol ratio of AM-to-AMPS-Na$^+$ was fixed at 15:85%. The amount of water in the polymerization was 10 ml. The effect of co-initiator content on equilibrium water absorbency of poly(AM-co-AMPS-Na$^+$) superabsorbent was investigated.

The effect of initiator (APS) from 0.6 to1.8 %mol of total monomer was studied at 0.05% mol of N-MBA, 0.6% mol of TEMED, and 10 ml of water. The effect of initiator content on equilibrium water absorbency of poly(AM-co-AMPS-Na$^+$) superabsorbent was investigated.

3.4.2   Synthesis of poly(AM-co-AMPS-Na$^+$)/fire retardant superabsorbent nano-composites

Synthesis of poly(AM-co-AMPS-Na$^+$)/mica superabsorbent nano-composite was synthesized using the same procedure as for the preparation of poly(AM-co-AMPS-Na$^+$) superabsorbent. The mol ratio of AM-to-AMPS-Na$^+$ was employed at 15:85%. Fire retardant was dispersed in the mixture of AM, AMPS-Na$^+$ and N-MBA (0.05% mol) in the presence of water at 10 ml using a half moon shape Teflon blade agitator for 60 min in the reactor. The investigated range of fire retardant content was from 5-30% wt. APS (0.6% mol) was added and stirred for   5   min   at 250 rpm at 60°C under nitrogen atmosphere, and subsequently TEMED (0.6% mol) was added. The mixture was stirred at 250 rpm for 30 min. The reaction was cooled

down to room temperature and the further step was done by following the same procedure described in Section 3.4.1 after the polymerization was stopped. Finally, the dried poly(AM-*co*-AMPS-Na⁺)/mica superabsorbent nanocomposites were obtained.

3.4.3 Synthesis of intercalating agent for modifying mica

Allyl bromide and 2-(dimethylamino)ethyl methacrylate were mixed in a 25 ml beaker at a 2:1 ratio by mmol for 5 min. The white powder of 2-methacryloxyethl allyldimethylammonium bromide intercalating agent was obtained in Scheme 3.1.

2-(dimethylamino)ethyl methacrylate

Allyl bromide

2-methacryloxyethyl allyldimethylamonium bromide
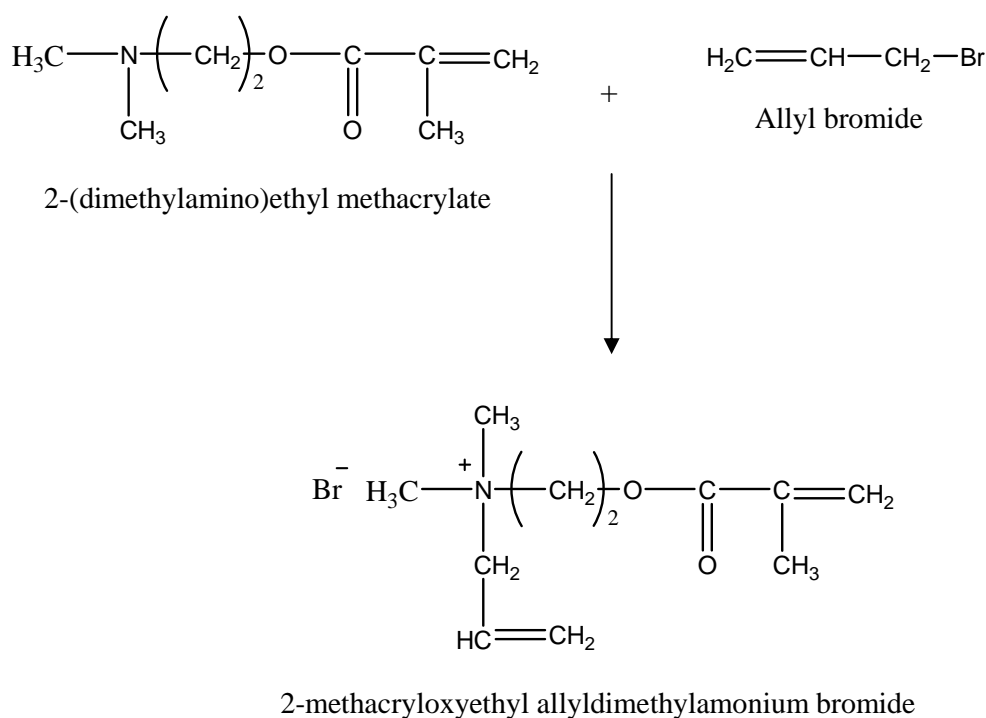
Scheme 3.1 Synthesis of 2-methacryloxyethyl allyldimethylammonium bromide

3.4.4 Synthesis of modified mica

Mica was dispersed in deionized water at the ratio of 1:8 w v^{-1}. The dispersion was stirred at 250 rpm for 1 h. An intercalating agent was then added in the mica dispersion and stirred for 24 h. The mica-to-the intercalating agent ratio was 1:1 w w^{-1}. The mixture was poured through a filter paper and subsequently dried for 24 h. The dry product was milled and sieved through a 100-mesh sieve. Finally, the modified mica was obtained. Thermal gravimetric analysis was employed to characterize the amount of intercalating agent in the modified mica.

3.4.5 Synthesis of poly(AM-*co*-AMPS-Na$^+$)/modified mica superabsorbent nanocomposites

Poly(AM-*co*-AMPS-Na$^+$)/modified mica superabsorbent nanocomposites were prepared using the same procedure as in Section 3.4.2 except the modified mica was used instead of the pristine mica.

3.5 Characterization

3.5.1 Identification of functional groups of poly(AM-*co*-AMPS-Na$^+$) and poly(AM-*co*-AMPS-Na$^+$)/mica nanocomposites

The functional groups of of poly(AM-*co*-AMPS-Na$^+$), poly(AM-*co*-AMPS-Na$^+$)/mica nanocomposites were characterized by Fourier Transform Infrared Spectroscopy (FTIR, Perkin Elmer, Spectrum GX, Massachusetts, USA) using a KBr pellet technique.

3.5.2 X-ray diffraction analysis of mica, modified mica and poly(AM-*co*-AMPS-Na$^+$)/mica nanocomposites

XRD patterns of the samples were recorded using Bruker AXS model D8 Discover (Bruker AXS Inc., Madison, Wisconsin, U.S.A) with Cu radiation,

voltage of 40 kV, a current of 40 mA with $\lambda = 0.15406$ nm, n = 1 and scanning range from 1-15° at 0.05°C min^{-1}. The interlayer spacing (d) of mica and mica-superabsorbent nanocomposites was calculated using Bragg's Equation (3.1):

$$n\lambda = 2d\sin\theta \qquad\qquad (3.1)$$

where d is the interplanar distance of the (001) reflection plane, θ is the diffraction angle, and λ is the wavelength.

3.5.3 Transmission electron microscopic analysis of poly(AM-*co*-AMPS-Na$^+$)/mica nanocomposites

TEM micrographs were taken using JOEL JEM-2100 (Jeol Ltd., Tokyo, Japan) under an accelerating voltage of 120 kV. The suspension was dropped onto a 300 mesh copper grid and dried in a control atmosphere before investigating TEM.

3.5.4 Thermal properties of SAPs and the nanocomposites

The thermal properties of poly(AM-*co*-AMPS-Na$^+$)/mica, poly(AM-*co*-AMPS-Na$^+$)/zinc borate, poly(AM-*co*-AMPS-Na$^+$)/melamine and poly(AM-*co*-AMPS-Na$^+$)/zinc borate/melamine nanocomposite were investigated by thermo-gravimetric analysis. TGA was investigated under nitrogen atmosphere at a heating rate of 20 °C min^{-1} from ambient temperature to 800 °C.

3.5.5 Water absorbency determination of SAPs and the nanocomposites

The equilibrium water absorbencies of SAPs and SAP nanocomposites were carried out in distilled water at room temperature. The dry product weighing 0.1 g was allowed to swell in the 200 cm^3 of deionized water for 24 h. The fully swollen superabsorbent polymers were then separated from the unabsorbed water by filtering

through a 100-mesh sieve aluminum screen for 2 h. The swollen superabsorbent polymers were weighed and the water absorbency at equilibrium (g g^{-1}) was calculated by Equation (3.2):

$$Equilibrium\ water\ absorbency = (W_s - W_d)/W_d \qquad (3.2)$$

where W_d = the weight of dry products (g), and W_s = the weight of the swollen gel (g). Water absorbency measurements were carried out in triplicate for each sample. The swelling kinetics of poly(AM-*co*-AMPS-Na$^+$)/mica, poly(AM-*co*-AMPS-Na$^+$)/zinc borate, poly(AM-*co*-AMPS-Na$^+$)/melamine were evaluated at 1, 3, 6, 12 and 24 h of swelling time.

3.5.6   Cone calorimetric analysis

According to ISO 5660, a cone calorimeter (Fire Testing Technology Ltd, UK) was employed at an incident heat flux (50 kW m^{-2}) in an air atmosphere, and under the free convective air flow condition. The SAPs were prepared in the form of an oil-in-water dispersion by adopting from Sortwell (2009) as follows.

The dry SAPs (40% w w^{-1}) were dispersed in a mixture of 50% w w^{-1} of palm oil and 10% w w^{-1} of nonionic surfactant blends having a net HLB value of 10 comprising 54% w w^{-1} of TWEEN 80/46% w w^{-1} of SPAN 80. The 5% v v^{-1} of SAPs in the oil was dispersed in deionized water, subsequently the viscous slurry gel was obtained. The SAP dispersion was then coated to give 3 mm thickness of SAP dispersion layer on a wood (Apocynaceae, Wrightia religiosa *Benth.*) board surface having a dimension of 100 x 100 x 3 mm^3. The surface of the SAP-coated wood specimen was exposed directly to an open flame generated by a propane gas jet. The uncoated wood board was also experimented as a control. The time to ignition, time

to burn through the coatings, and time to burn through the board were recorded. The charred samples left from the experiments were recorded by a digital camera (Canon PowerShot A630, Canon (China) Co Ltd, Beijing China) after the specimen was ignited into flame.

CHAPTER IV

RESULTS AND DISSCUSION

4.1 Synthesis of acrylamide-based copolymeric superabsorbents: Effect of acid and salt forms of the ionic monomer

Copolymeric superabsorbents of acrylamide and ionic monomer were synthesized by crosslinking solution polymerization. In this study, the effects of acid and salt forms of the selected ionic monomers (2-acrylamido-2-methylpropane sulfonic acid and its respective sodium salt) on water absorbency of the prepared SAPs were investigated. Existence of the newly synthesized SAPs was identified via an FTIR spectroscopic technique.

4.1.1 Identification of existence of poly(AM-*co*-AMPS-H$^+$) and poly(AM-*co*-AMPS-Na$^+$) superabsorbents

In Figure 4.1 and Table 4.1, the superabsorbent composites were characterized by FTIR technique. The spectrum (a) in Figure 4.1 shows a strong peak of N-H stretching at 3342 cm^{-1}, a strong peak of the =C-H stretching at 3161 cm^{-1} and a sharp peak of C=O stretching at 1670 cm^{-1} (Tang *et al.*, 2008), which are the components of acrylamide. The spectrum (b) shows one strong peak of the C=O stretching of amide I at 1651 cm^{-1} and a sharp peak of the S=O group of AMPS-Na$^+$ at 1043 cm^{-1} (Durmaz and Okay, 2000). The spectrum (c) shows another strong peak of the C=O stretching of amide I at 1637 cm^{-1}, a strong peak of the N-H bending of amide II at 1542 cm^{-1} and the sharp peak of the S=O stretching of AMPS-H$^+$ at 1037 cm^{-1} (Lin *et al.*, 2008).

Table 4.1 Assignments for FTIR spectrum of acrylamide, poly(AM-*co*-AMPS- Na$^+$) and poly(AM-*co*-AMPS-H$^+$)

Sample	Wave number (cm^{-1})	Assignments
Acrylamide	3342	N-H, O-H stretching
	3161	=C-H stretching
	1670, 1610	C=O stretching of amide I
	1427	N-H bending of amine
	1280	C-N stretching
Poly(AM-*co*-AMPS- Na$^+$)	3396-3330	N-H, O-H stretching
	2977, 2929	C-H stretching of CH, CH$_2$
	1651	C=O stretching of amide I
	1542	N-H bending of amide II
	1043	S=O stretching
Poly(AM-*co*-AMPS- H$^+$)	3308-3178	N-H, O-H stretching
	2989, 2914	C-H stretching of CH, CH$_2$
	1637	C=O stretching of amide I
	1542	N-H bending of amide II
	1037	S=O stretching
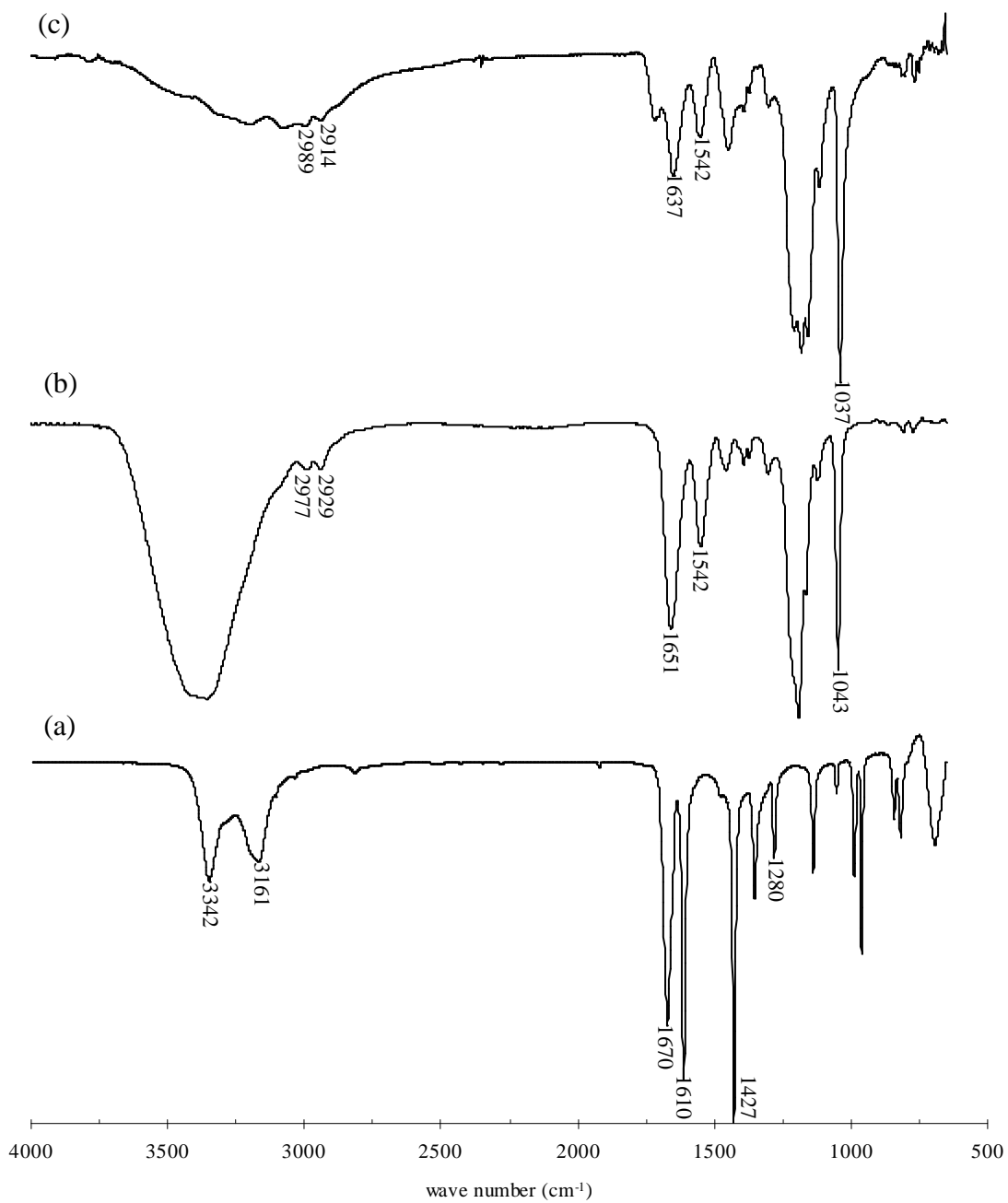
Figure 4.1 FTIR spectra of (a) acrylamide and (b) poly(AM-*co*-AMPS- Na$^+$) and (c) poly(AM-*co*-AMPS-H$^+$)

4.1.2 Effect of ionic comonomer on water absorbency

Water absorbency of all the SAP samples is shown in Figure 4.2 and Table 4.2. The equilibrium water absorbency of poly(AM-*co*-AMPS-Na$^+$) was found to increase abruptly from 60 g g^{-1} to 244 g g^{-1} when the content of AMPS-Na$^+$ in the synthesis ingredient was increased from 2 to 10% mol (Figure 4.2). Beyond this content, the water absorbency increased continuously until it reached a maximum absorption at 967 g g^{-1} by 85% mol of AMPS-Na$^+$. The increase in water absorbency corresponds to increases in the ionic group content (the sulfonate groups) in the superabsorbent polymers so prepared. Further increases in AMPS-Na$^+$ loading beyond 85% mol yielded a slurry product.
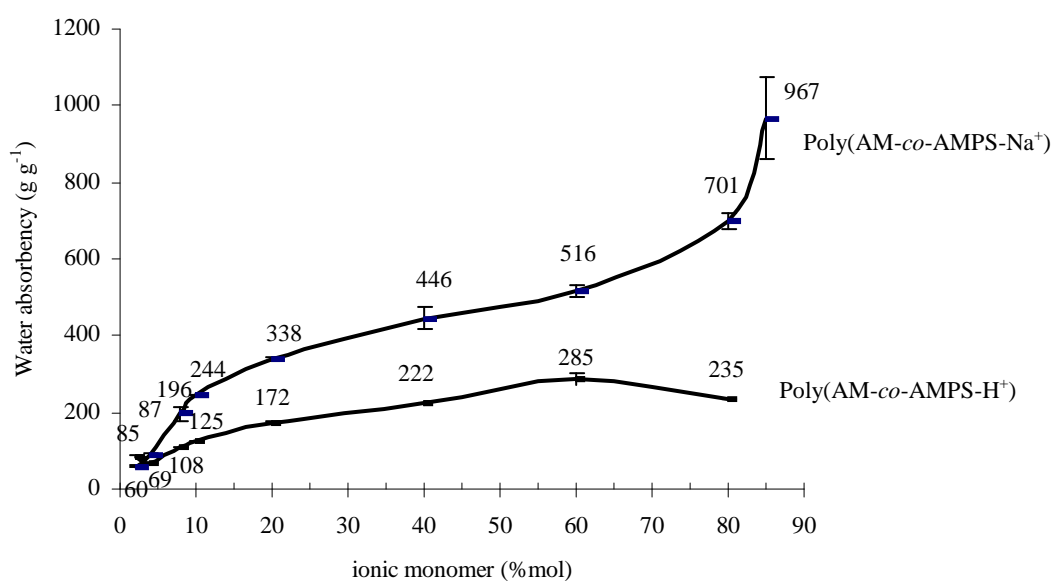
Figure 4.2 Effect of ionic comonomer on equilibrium water absorbency of the copolymeric superabsorbents synthesized with AM: ionic monomer mol ratios from 98:2 to 15:85, N-MBA, APS, and TEMED contents at 0.2, 1.2, and 1.2% mol, respectively.

By adopting the proposed model (Buchholz and Burgert, 2006), we can postulate the swelling mechanism of the superabsorbent polymer as already shown in

Figure 2.3. The superabsorbent polymer consists of many hydrophilic polymer chains with the sulfonate groups and crosslinking points between the chains to prevent an infinite swelling. The dissociated sodium sulfonate groups increase osmotic pressure inside the polymer. The negative charges of the sulfonate groups repel one another to expand the polymer coils and are compensated by the positive charges of sodium salt. When the polymer is in contact with water, water diffuses into the polymer network and then solvates the sodium ions and the negatively charged sulfonates. The driving force for swelling is the difference between the osmotic pressure inside and outside the polymer. Likewise, the equilibrium water absorbency of poly(AM-*co*-AMPS-H$^+$) increased rather idly with the content of AMPS-H$^+$. Therefore, its absorption is less than that of poly(AM-*co*-AMPS-Na$^+$) at the same content of ionic comonomer (Figure 4.2). Swelling mechanism of the superabsorbent polymers is previously illustrated in Figure 2.3. Based on the mechanism, the higher water absorbency of poly(AM-*co*-AMPS-Na$^+$) can be explained by three attributes: 1) the presence of salt form (AMPS-Na$^+$) yields a higher difference in ionic osmotic pressures between the hydrogel and the swelling medium, H$_2$O; 2) the larger Na$^+$ ions trapped in the superabsorbent can induce the copolymer chain; 3) the strong acidity of AMPS-H$^+$ might induce a chain scission reaction (Odian, 2004) in the copolymer prepared. Therefore, for this ionic monomer, the salt form (AMPS-Na$^+$) was chosen to copolymerize with AM (nonionic monomer) since the prepared poly(AM-*co*-AMPS-Na$^+$) superabsorbent provided the larger water absorbency comparative to the superabsorbent of poly(AM-*co*-AMPS-H$^+$).

Table 4.2 Effect of components on equilibrium water absorbency of poly(AM-*co*-AMPS-Na$^+$) superabsorbents

AM-to- ionic comonomer molar ratio	Equilibrium water absorbency (g g^{-1})	
	AMPS-Na$^+$	AMPS-H$^+$
98:2	60±3	85±3
96:4	87±5	69±1
92:8	196±16	108±3
90:10	244±1	125±1
80:20	338±4	172±6
70:30	367±12	N/A
60:40	446±31	222±1
50:50	460±24	N/A
40:60	516±14	285±16
30:70	520±8	N/A
20:80	701±21	235±2
15:85	967±104	N/A

N/A = was not synthesized

4.2 Synthesis of poly(AM-*co*-AMPS-Na$^+$) SAPs: Effect of the degree of monomer dilution, and the contents of crosslinker, co-initiator, and initiator on water absorbency

4.2.1 Effect of the amount of crosslinker and the degree of monomer dilution on water absorbency

Effects of the amount of N-MBA crosslinker and the degree of monomer dilution on water absorbency were studied. Different amounts of crosslinker ranging from 0.05-0.2% mol were investigated. Effect of the degree of monomer dilution on water absorbency was studied by varying the amount of reaction medium (water) in the polymerization. In this study, two levels of water content (10 and 40 ml) were investigated. The degrees of equilibrium water absorbency of poly (AM-*co*-AMPS-Na$^+$) as functions of the amount of crosslinker and water present in the polymerization are shown in Table 4.3 and Figure 4.3. The SAPs were synthesized from 15:85 mol ratio of AM: AMPS-Na$^+$, 1.2% mol of APS and 1.2% mol of TEMED.

Table 4.3 Effect of crosslinker and DI water contents in the polymerization on equilibrium water absorbency of poly(AM-*co*-AMPS-Na$^+$) superabsorbents

N-MBA (% mol)	Equilibrium DI water absorbency (g g^{-1}) at reaction medium	
	10 ml	40 ml
0.05	1006±95	N/A
0.10	746±26	N/A
0.20	399±31	967±104

N/A = could not be measured due to the slurry product obtained
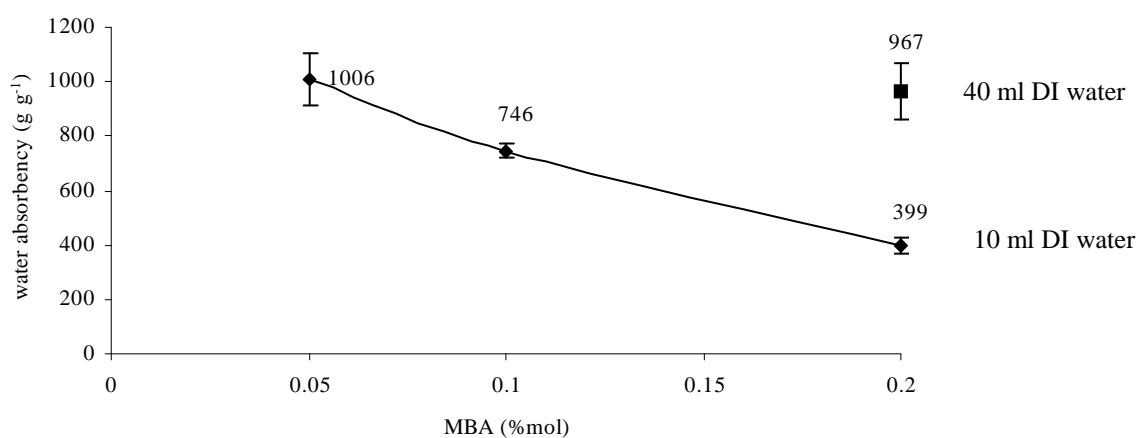
Figure 4.3 Effect of crosslinker contents on equilibrium water absorbency of poly(AM-*co*-AMPS-Na$^+$) superabsorbents synthesized with AM-to-AMPS-Na$^+$ ratios at 98:2 to 15:85, APS and TEMED contents at 1.2 and 1.2 %mol of total monomers, by 10 ml DI water and 40 ml DI water

The results in Table 4.3 indicate that the equilibrium water absorbency of poly(AM-*co*-AMPS-Na$^+$) decreased inversely proportional to the N-MBA content

because crosslinking agent involved directly with the degree of crosslinking density. Increasing the crosslinker content shortens the molecular weight of polymer between crosslinking junctions, as a result, the decrease in chain flexibility and the limited chain expansion during the swelling of SAPs were observed.

Equilibrium water absorbency of poly(AM-*co*-AMPS-Na$^+$) increased in relation to the degree of monomer dilution or the increase in medium content (water) in the polymerization reaction. As seen in Table 4.3, at 0.2% mol of N-MBA, the polymerization system with 40 ml of water produced the SAPs with larger water absorbency. The reason can be that the higher water in the polymerization decreases the crosslinker concentration in the system to probably decreasing crosslinking positions in polymer chain to generate the greater chain flexibility. However, at the N-MBA content lower than 0.2% mol, the obtained product after polymerization did not form a gel structure due to the very dilute polymerization system and the low content of crosslinker (Travas-Sejdic and Easteal, 2000).

4.2.2 Effects of amounts of co-initiator and initiator

The equilibrium water absorbencies of poly(AM-*co*-AMPS-Na$^+$) superabsorbents synthesized with AM:AMPS-Na$^+$ mol ratio of 15:85, 0.05% mol of N-MBA with various contents of the co-initiator (TEMED) and initiator (APS) are shown in Tables 4.4 and Figure 4.4, Table 4.5 and Figure 4.5, respectively.

Table 4.4 Effect of TEMED contents on equilibrium water absorbency of poly(AM-*co*-AMPS-Na$^+$) superabsorbents*

TEMED (% mol)	equilibrium water absorbency (g g^{-1})
0.6	981±8
1.2	983±74
1.8	1006±95
2.4	N/A

*APS content = 1.2% mol

N/A = could not be measured due to the slurry product obtained

Table 4.5 Effect of APS contents on equilibrium water absorbency of poly(AM-*co*-AMPS-Na$^+$) superabsorbents*

APS (% mol)	equilibrium water absorbency (g g^{-1})
0.6	1212±54
1.2	981±8
1.8	797±85

*TEMED content = 0.6% mol
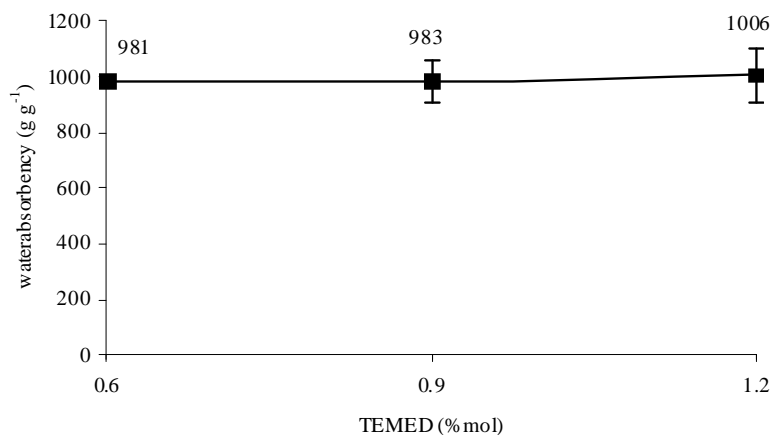
Figure 4.4 Effect of TEMED contents on equilibrium water absorbency of poly(AM-*co*-AMPS-Na$^+$) superabsorbents synthesized with AM-to-AMPS-Na$^+$ ratios at 15:85, 1.2% mol APS, 0.05% mol N-MBA and 10 ml deionized water
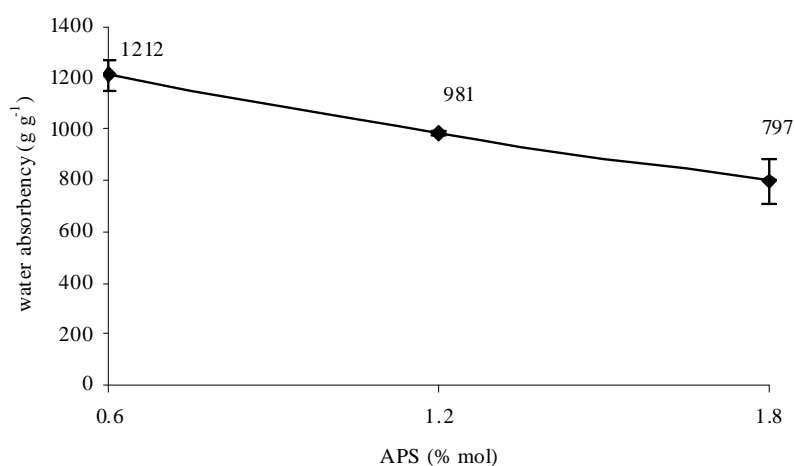
Figure 4.5 Effect of APS contents on equilibrium water absorbency of poly(AM-*co*-AMPS-Na$^+$) superabsorbents synthesized with AM-to-AMPS-Na$^+$ ratios at 15:85, 0.6 %mol TEMED, 0.05% mol N-MBA and 10 ml deionized water

As shown in Table 4.4 and Figure 4.4, TEMED plays a role on water absorbency of the prepared SAPs. The equilibrium water absorbency slightly increased with the increasing TEMED content. In a redox initiated polymerization, i.e. the APS and TEMED pair, TEMED functions as a reducing agent to generate an electron to reduce the APS, an oxidizing agent. TEMED accelerates and generates a longer number of free radicals to give optimal chain lengths with flexibility; therefore,

the water absorbency was enhanced. However, when TEMED concentration was low, no sufficient hydroxyl radicals were generated. Thus, short polymer chains were produced, resulting in the low water absorbency of the superabsorbents. Besides, TEMED is a strong base, so it may hydrolyze or neutralize the sulfonate groups to enhance water absorption.

The effect of initiator content (APS) on water absorbency is shown in Table 4.5 and Figure 4.5. The equilibrium water absorbency increased with decreasing APS content. At the low content of APS, the number of generated propagating chains was low. Therefore, the prepared SAPs with the longer polymer chains were produced, yielding the product with high water absorbency as comparative to the system synthesized from high content of APS.

The results showed that the maximum equilibrium water absorbency at 1212 ± 54 g g^{-1} was obtained from poly(AM-*co*-AMPS-Na$^+$) synthesized with AM:AMPS-Na$^+$ mol ratio of 15:84%, 0.05% mol of N-MBA, 0.6% mol of APS, 0.6% mol of TEMED, and 10 ml of the reaction medium (water). Therefore, in the next section, this formulation was employed to prepare SAP composites in order to provide SAPs with a high amount of water absorbency and good thermal stability.

4.3   Synthesis of poly(AM-*co*-AMPS-Na$^+$)/mica superabsorbent composites

Besides the high water absorbency, thermal stability is also another important property for fire retardants. The mixed superabsorbent composite with mica (0.30% w w^{-1}) and *in situ* polymerized superabsorbent composite were thus carried out.

4.3.1   Identification of functional group of mica and poly(AM-*co*-AMPS-Na$^+$)/mica superabsorbent composites

The spectrum (a) in Figure 4.6 and the assignments in Table 4.6 show a strong peak of Si-O stretching at 972 cm^{-1} and a sharp peak of Al-O stretching at 694 cm^{-1} (Dai *et al*., 2006), which confirm the pristine mica. The spectra (b), (c), (d) and (e) show the overlapping broad peaks of N-H stretching and O-H stretching at 3418 cm^{-1} and 3307 cm^{-1}, the strong peak of C=O stretching of amide I at 1641 cm^{-1} (Tang *et al*., 2008), the strong peak of the C=O stretching of amide I at 1651 cm^{-1}, the sharp peak of the S=O group of AMPS-Na$^+$ at 1043 cm^{-1} (Durmaz and Okay, 2000) and peak of the Si-O stretching at 972 cm^{-1} being increased in relate to the amount of mica loaded in the synthesized composites. The results indicated that the resulting products were the desired SAP composite.
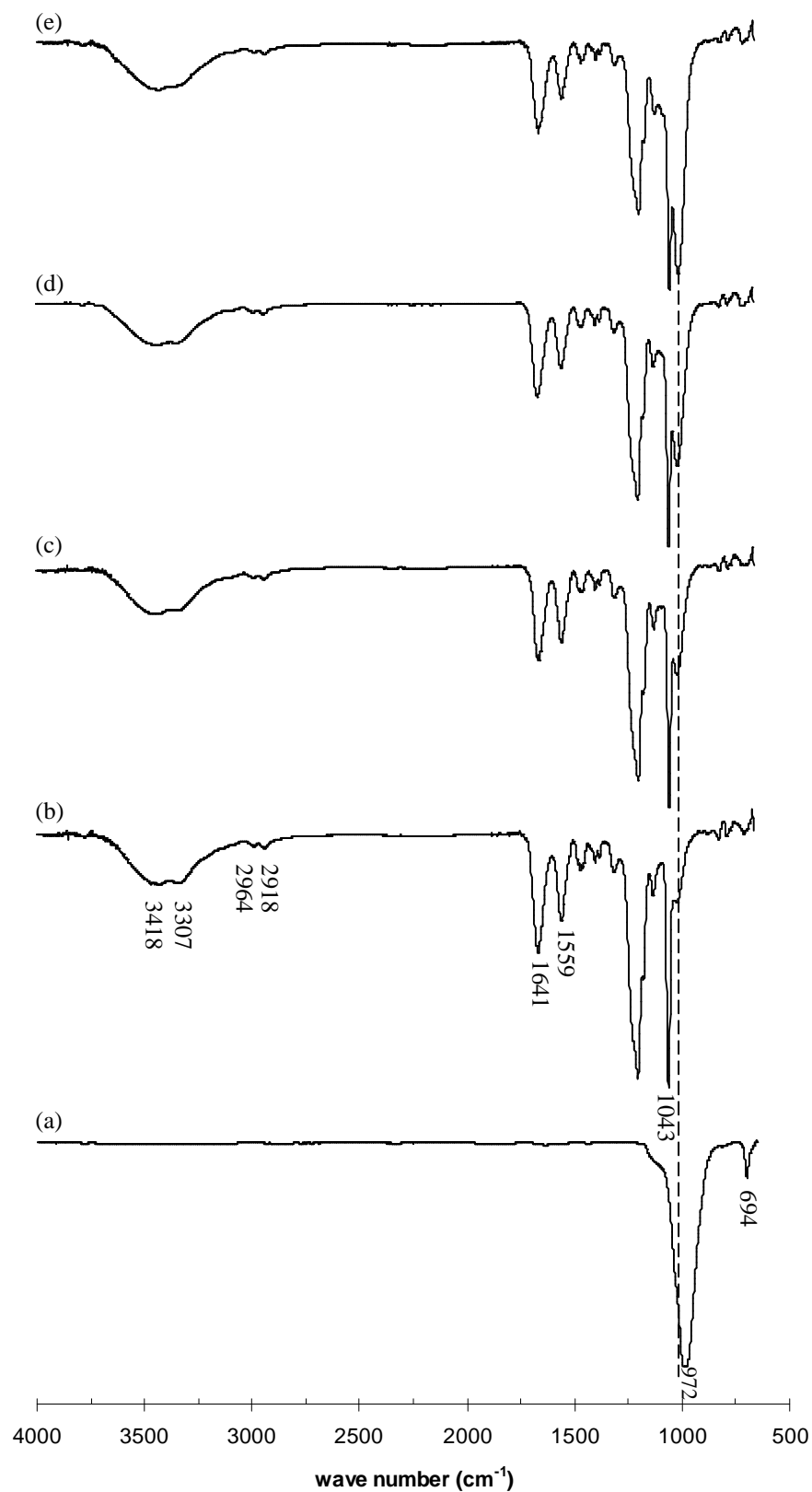
Figure 4.6 FTIR spectra of (a) pristine mica, and poly(AM-*co*-AMPS-Na⁺)/mica nanocomposites with various mica contents of (b) 5%, (c) 10%, (d) 20%, and (e) 30% w w⁻¹. (All superabsorbents were prepared with AM: AMPS-Na⁺ mol ratio of 15: 85, 0.05% mol of N-MBA, 0.6% mol of APS, and 0.6% mol of TEMED)

Table 4.6 Assignments for FTIR spectra of mica, and poly(AM-*co*-AMPS-Na$^+$)/mica nanocomposites

Sample	Wave number (cm^{-1})	Assignments
Mica	972	Si-O stretching
	694	Al-O stretching
Poly(AM-*co*-AMPS-Na$^+$)/mica	3418-3307	N-H, O-H stretching
	2964, 2918	C-H stretching of CH, CH$_2$
	1641	C=O stretching of amide I
	1559	N-H bending of amide II
	1043	S=O stretching

4.3.2 X-ray diffraction of mica and poly(AM-*co*-AMPS-Na$^+$)/mica superabsorbent nanocomposites

The basal spacing (d-spacing) of mica and poly(AM-*co*-AMPS-Na$^+$)/mica nanocomposites were investigated by X-ray diffraction. The XRD pattern of mica in Figure 4.7 illustrates the characteristic peaks at 2-theta = 7.2 and 9.2 corresponding to the basal spacing of 12.4 and 9.6Å, respectively. The neat poly(AM-*co*-AMPS-Na$^+$) superabsorbent (Figure 4.8(a)) does not exhibit the characteristic peaks as observed in the rest of Figure 4.8. When 5 %w w^{-1} mica was dispersed in the polymerization reaction of poly(AM-*co*-AMPS-Na$^+$) (Figure 4.8(b)), the 2-theta of mica in the nanocomposite shifted toward the lower angles (2-theta = 6.4 degrees, d-spacing = 13.9 Å in Figure 4.84.8(b)), compared with the pure mica (2-

theta = 7.2 degrees, d-spacing = 12.4 Å in Table 4.7). This result confirms that poly(AM-*co*-AMPS-Na$^+$)/mica nanocomposites having the intercalated structure were confirmed. There are some increases in the 2-theta when increasing the mica content to 10-30% w w^{-1} which indicates that the interlayer distance of mica (from 13.9-13.1 Å) decreases (Figure 4.8 and Table 4.7).
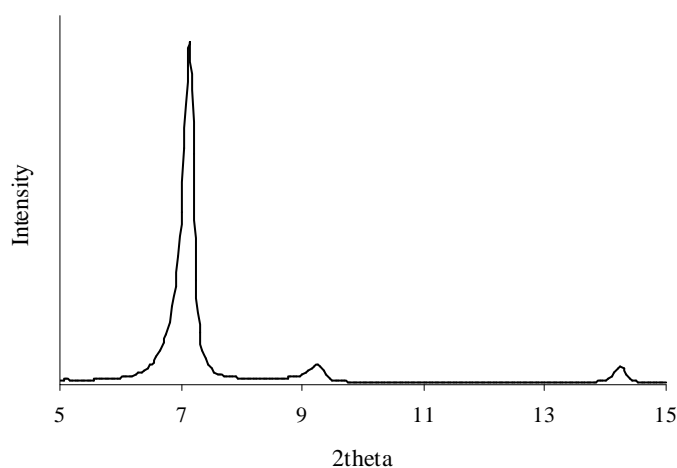
Figure 4.7 X-ray diffraction patterns of pristine mica
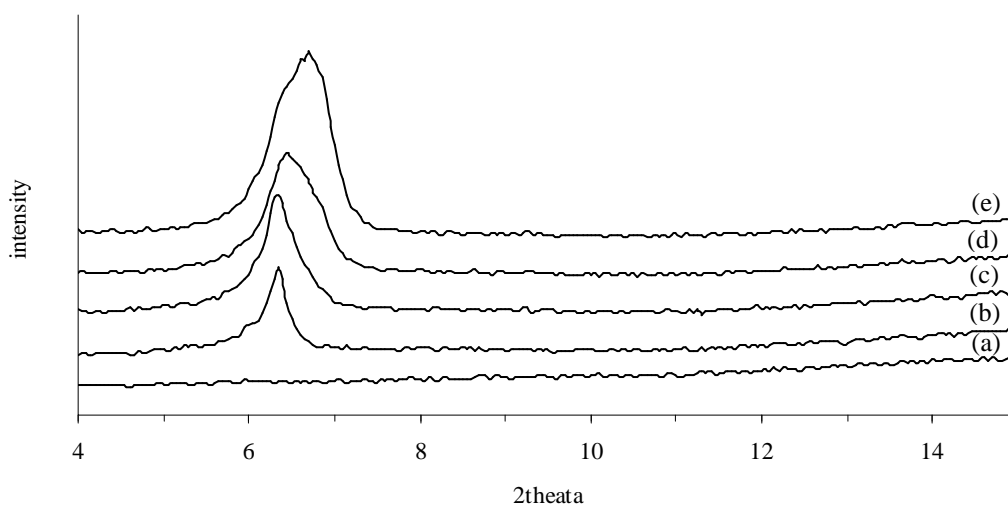
Figure 4.8 X-ray diffraction patterns of (a) poly(AM-*co*-AMPS-Na$^+$) superabsorbents and poly(AM-*co*-AMPS-Na$^+$)/mica nanocomposite with various mica contents of (b) 5%, (c) 10%, (d) 20%, and (e) 30% w w^{-1}. (All superabsorbents were prepared with AM : AMPS-Na$^+$ mol ratio of 15 : 85, 0.05 % mol of N-MBA, 0.6% mol of APS, and 0.6% mol of TEMED)

Table 4.7 2-theta and the calculated basal spacing of mica and poly(AM-*co*-AMPS-Na$^+$)/mica nanocomposites with various amounts of mica addition

Mica (% w w^{-1})	2-theta	d$_{001}$(Å)
Pristine Mica	7.2	12.4
	9.2	9.6
5	6.4	13.9
10	6.4	13.9
20	6.5	13.7
30	6.6	13.1

4.3.3   TEM micrographs poly(AM-*co*-AMPS-Na$^+$)/mica superabsorbent nanocomposites

To confirm the intercalated structure of the prepared nanocomposites, TEM was employed to characterize the morphology. TEM analysis is usually used to support the XRD result by visualizing the dispersion of mica in the nanometer scale. The TEM micrographs of poly(AM-*co*-AMPS-Na$^+$)/mica nanocomposites with different contents of mica (5 - 30 %w w^{-1}) are shown in Figures 4.9 (a-d). The dark lines of mica in the bright matrix of the superabsorbents are observed. It was found that during the polymerization mica was *in situ* intercalated by the polymerizing monomers which were then polymerized to form the superabsorbents matrix. In Figure 4.9, the silicate layers of mica were dispersed in the superabsorbent matrix and formed the intercalated structure at a nanometer scale in the superabsorbent matrix. All TEM micrographs of the nanocomposites show the distance between the two adjacent dark lines corresponding to the spacing of the two silicate layers obtained

from XRD data. Based on the results from XRD and TEM, it is possible to confirm that poly(AM-*co*-AMPS-Na$^+$)/mica nanocomposites had an intercalated structure.
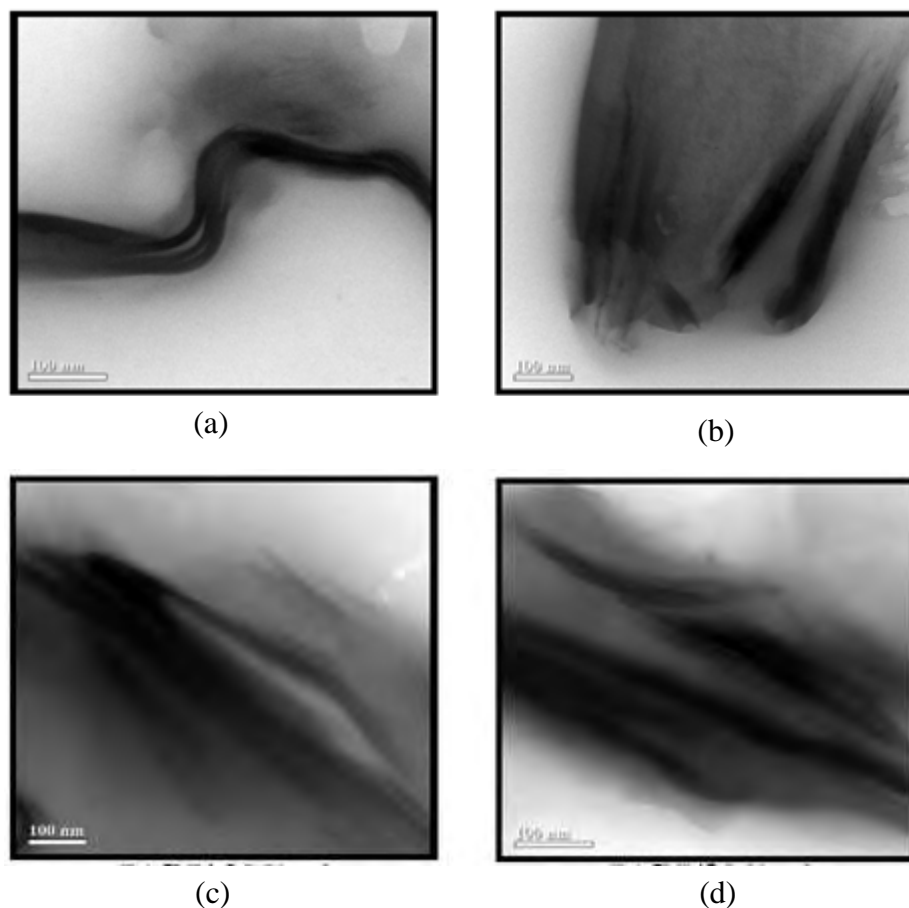
Figure 4.9 TEM micrographs of poly(AM-*co*-AMPS-Na$^+$)/mica nanocomposites with various mica contents of: (a) 5%, (b) 10%, (b) 20% and (d) 30% w w^{-1}

4.3.4 Effect of mica contents on water absorbency of poly(AM-*co*-AMPS-Na$^+$)/mica superabsorbent nanocomposites

Figure 4.10 shows water absorbency of all mica contents in superabsorbent nanocomposites. During the 0-3 h swelling time, water absorbency rapidly increased and reached equilibrium water absorbency at 6 h in all

superabsorbent nanocomposites. In same swelling time, water absorbency was decreased when increasing mica content.
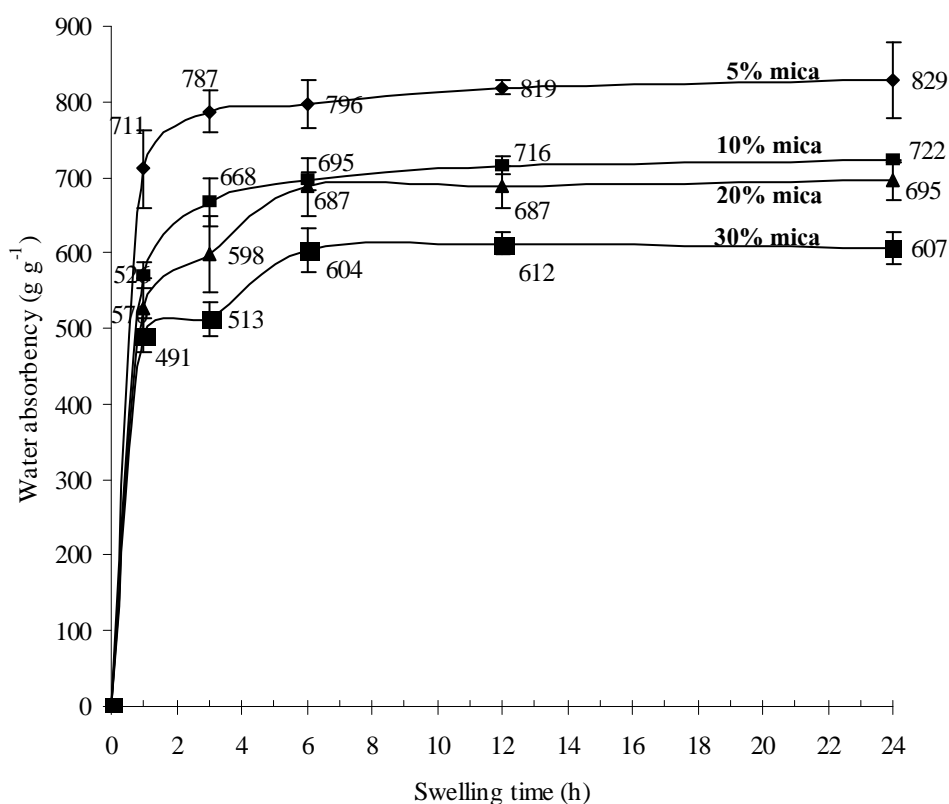
Figure 4.10 Deionized water absorbency of mica incorporated superabsorbent nanocomposits (SAPC) at various swelling times

The water absorbencies of the poly(AM-*co*-AMPS-Na$^+$)/mica superabsorbent nanocomposites synthesized with various contents of mica addition are shown in Figure 4.11. The result also indicates that with increasing mica content the water absorbency decreases. The pronounced reduction in water absorbency was found when 5%w w^{-1} of mica was added. Beyond this value, the continuous reduction of water swelling was observed. The presence of mica in the SAPs acts as a physical crosslink junction within the composite in which the polymer chain intercalated within the layers of mica, thus, reducing the water absorbency in proportional to the content of mica (Foungfung *et al.*, 2010).
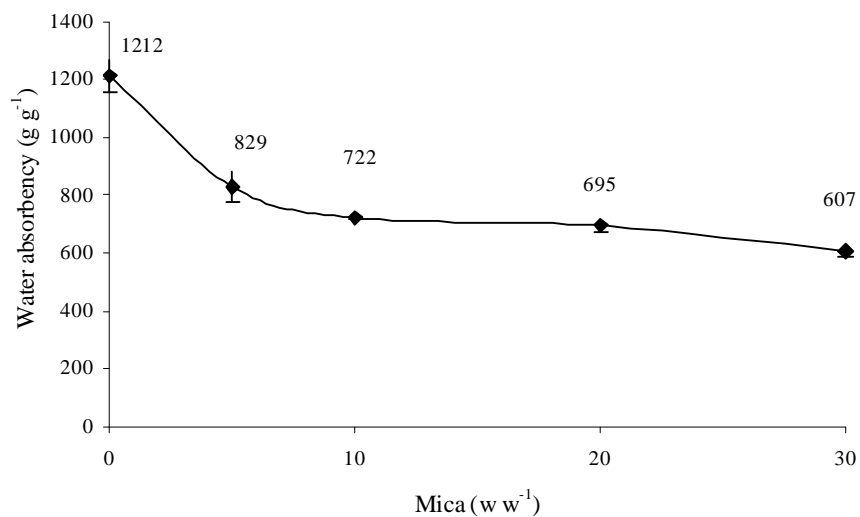
Figure 4.11 Effect of mica content on equilibrium water absorbency of poly(AM-*co*-AMPS-Na^{+})/mica superabsorbent nanocomposites as a function of mica content

4.4 Synthesis of modified mica

4.4.1 X-ray diffraction of mica and modified mica

Figure 4.12 shows the XRD patterns of mica and 2-methacryloyloxyethyl allyldimethylammonium bromide (MHAB)-modified mica. The modification of mica via interaction with MHAB expanded the width of the basal spacing of the modified mica from 12.4 Å to 13.9 Å.
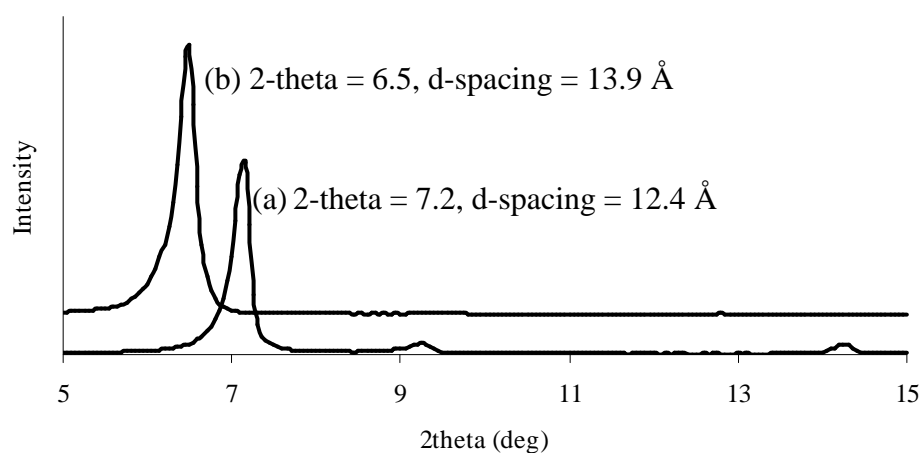
Figure 4.12 X-ray diffraction patterns of (a) pristine mica, and (b) MHAB-modified mica

4.4.2 Effect of the modified mica on equilibrium water absorbency of poly(AM-*co*-AMPS-Na$^+$) superabsorbents

The amounts of the modified mica investigated by the TGA technique are presented in Figure 4.13, in which the MHAB loading of the modified mica is 11.78% w w^{-1} of pristine mica obtained by calculating the amount of double bond of the crosslinking agent and intercalating agent represent in the modified mica which was found 6.47×10^{-4} mol g^{-1}.

The equilibrium water absorbency of the poly(AM-*co*-AMPS-Na$^+$)/modified mica superabsorbent nanocomposites synthesized with various modified mica loadings cannot be obtained. These products were the soluble gel because the double bonds of intercalating agent could not be completed and it was unstable in water, and the monomers in polymerization were obstructed by the steric of MHAB in mica interlayer. Therefore, the calculated amount of double bonds was lower than the reacted amount.

Weight loss (%) vs Temperature (^{0}C)
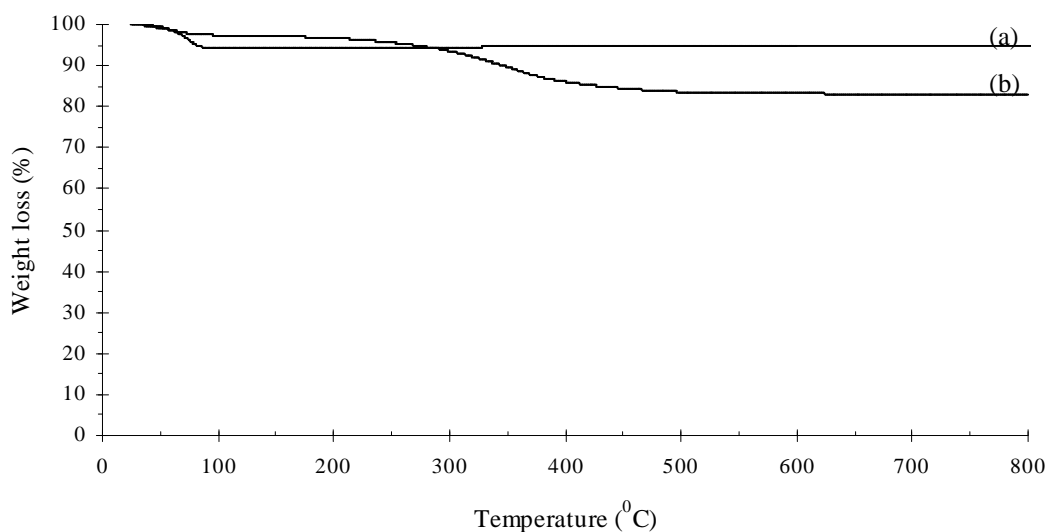
Figure 4.13 TGA thermograms of (a) mica, (b) modified mica

Besides the high swelling capacity, the superabsorbents used in fire retardant application should have a good thermal property. The SAP/mica nano-composites, containing other fire retardant agents of zinc borate and melamine were prepared to improve the gel thermal stability.

4.5 Characterization of poly(AM-*co*-AMPS-Na$^+$)/fire retardant super-absorbent nanocomposites

4.5.1 Identification of functional group of superabsorbent nanocomposites

4.5.1.1 Zinc borate and poly(AM-co-AMPS-Na$^+$)/zinc borate superabsorbent nanocomposites

The spectrum (a) in Figure 4.14 shows a strong peak of the asymmetric B(3)-O stretching at 1406 cm^{-1} and a sharp peak of B(4)-O stretching at 1090 and 798 cm^{-1} (Yongzhong *et.al.*, 1999). The spectra (b), (c), (d) and (e) show the overlapping broad peaks of N-H stretching and O-H stretching at 3418 cm^{-1} and 3307

cm^{-1}, respectively; the strong peak of C=O stretching of amide I at 1641 cm^{-1} (Tang *et al.,* 2008), the strong peak of N-H blending of amide II at 1559 cm^{-1} and the sharp peak of the S=O group of AMPS-Na$^+$ at 1043 cm^{-1} (Durmaz and Okay, 2000) and peak of the B(4)-O stretching at 1090 cm^{-1}. The peak of B(4)-O was increased in relation to the amount of zinc borate added in the synthesized composites (Table 4.8).
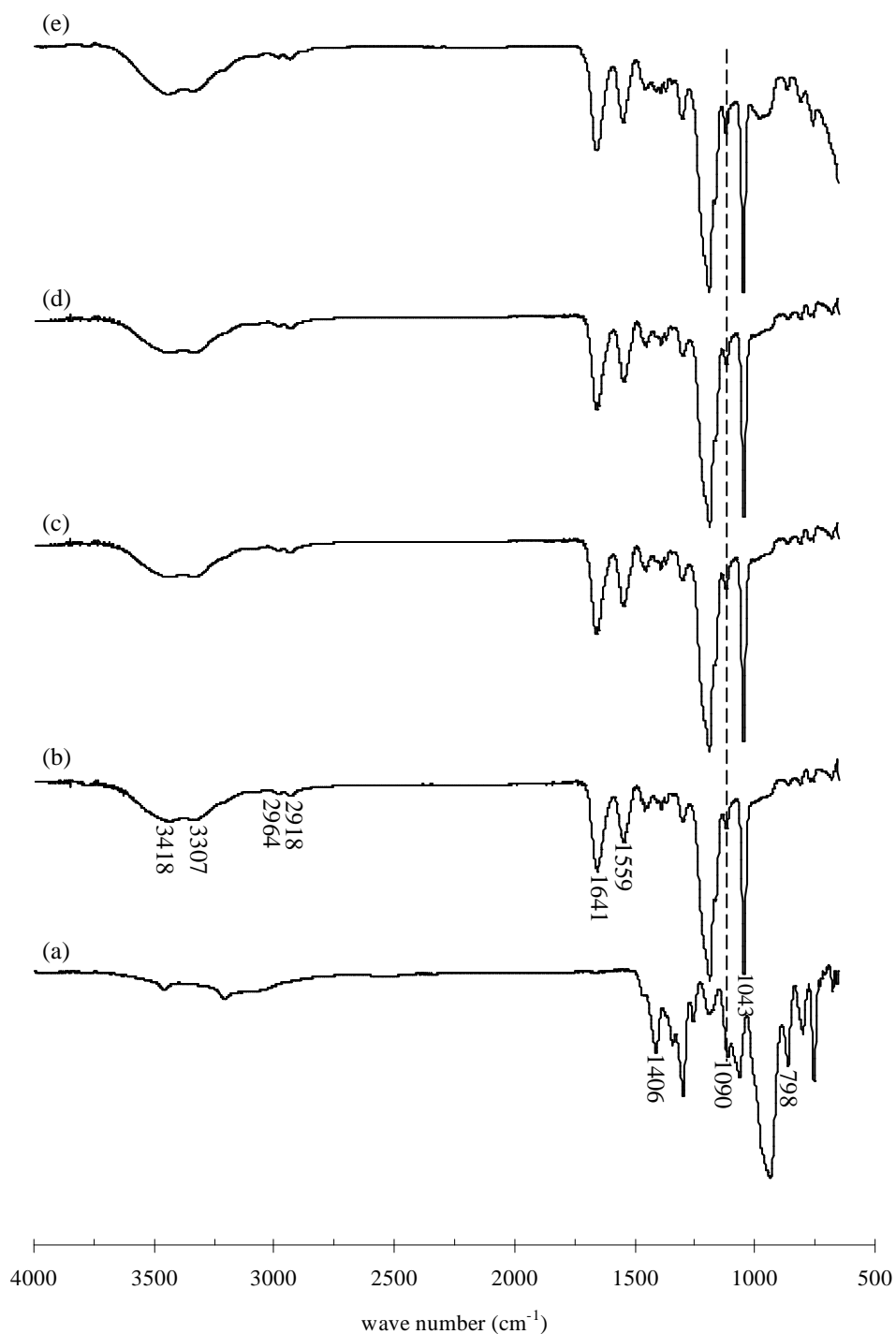
Figure 4.14 FTIR spectra of (a) zinc borate, and poly(AM-*co*-AMPS-Na$^+$)/zinc borate nanocomposite with various zinc borate contents of (b) 5%, (c) 10%, (d) 20%, and (e) 30% w w^{-1}. (All superabsorbents were prepared with AM: AMPS-Na$^+$ mol ratio of 15: 85, 0.05% mol of N-MBA, 0.6% mol of APS, and 0.6% mol of TEMED)

Table 4.8 Assignments for FTIR spectrum of zinc borate, and poly(AM-*co*-AMPS-Na$^+$)/zinc borate nanocomposites

Sample	Wave number (cm^{-1})	Assignments
Zinc borate	1406	B(3)-O stretching
	1090, 798	B(4)-O stretching
Poly(AM-*co*-AMPS-Na$^+$)/zinc borate	3418-3307	N-H, O-H stretching
	2964, 2918	C-H stretching of CH, CH$_2$
	1641	C=O stretching of amide I
	1559	N-H bending of amide II
	1043	S=O stretching

4.5.1.2 Melamine and poly(AM-co-AMPS-Na$^+$)/melamine superabsorbent nanocomposites

The spectrum (a) in Figure 4.15 shows strong peaks of the N-H stretching at 3468, 3414 and 3312 cm^{-1}, the strong peak of C=O stretching at 1647 cm^{-1}, the shape peak of C-N stretching at 1433 cm^{-1} and sharp peak of C-O stretching at 1186 cm^{-1} (Hu *et.al*., 2006). The spectra (b) to (e) show the overlapping broad peak of N-H stretching and O-H stretching at 3418 cm^{-1} and 3307 cm^{-1}, the strong peak of C=O stretching of amide I at 1641 cm^{-1} (Tang *et al*., 2008), the strong peak of N-H blending of amide II at 1559 cm^{-1} and the sharp peak of S=O group of AMPS-Na$^+$ at 1043 cm^{-1} (Durmaz and Okay, 2000) and peak of the N-H stretching at 3468 - 3312

cm^{-1} increased in relation to the amount of melamine in the synthesized composites (Table 4.9).
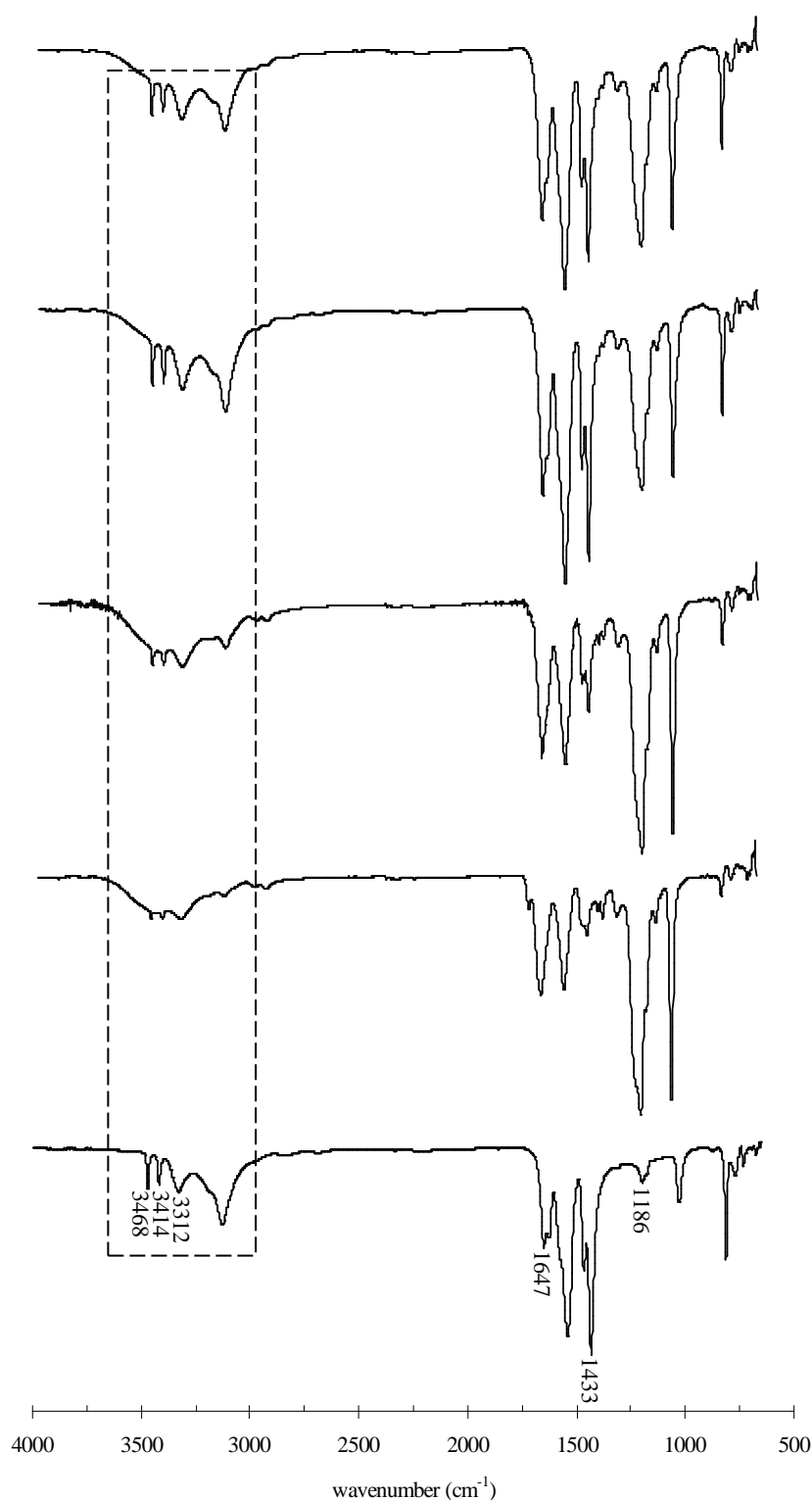
Figure 4.15 FTIR spectra of (a) melamine and poly(AM-*co*-AMPS-Na$^+$)/melamine nanocomposite with various melamine contents of (b) 5%, (c) 10%, (d) 20% and (e) 30% w w^{-1}. (All superabsorbents were prepared with AM:AMPS-Na$^+$ mol ratio of 15: 85, 0.05% mol of N-MBA, 0.6% mol of APS, and 0.6% mol of TEMED)

Table 4.9 Assignments for FTIR spectrum of melamine, and poly(AM-*co*-AMPS-Na⁺)/melamine nanocomposites

Sample	Wave number (cm⁻¹)	Assignments
Melamine	3468, 3414, 3312	N-H bending of melamine
	1647	C=O stretching of amide I
	1433	C-N stretching
	1186	C-O stretching
Poly(AM-*co*-AMPS-Na⁺)/melamine	3418-3307	N-H, O-H stretching
	2964, 2918	C-H stretching of CH, CH$_2$
	1641	C=O stretching of amide I
	1559	N-H bending of amide II
	1043	S=O stretching

4.5.2 Swelling kinetic of poly(AM-*co*-AMPS-Na⁺)/zinc borate superabsorbent nanocomposites

The superabsorbents/zinc borate nanocomposites prepared from zinc borate loadings of 5, 10, 20 and 30% w w⁻¹ of the monomer. Deionized water absorbency in Figure 4.16 relatively reached the swelling equilibrium after 6 h of swelling. The prepared zinc borate polymer nanocomposites had lower equilibrium water absorbency as compared to the neat SAPs (1212±54 g g⁻¹). Moreover, the equilibrium water absorbency of poly(AM-*co*-AMPS-Na⁺)/zinc borate nanocom-

posites decreased with increasing zinc borate loadings. This could be due to the presence of zinc borate in the SAP matrix to reduce polarity and osmotic pressure of the SAPCs during the swelling. The excess amount of 30 %w w^{-1} zinc borate could not be completely incorporated in the polymer matrix during the polymerization reaction.
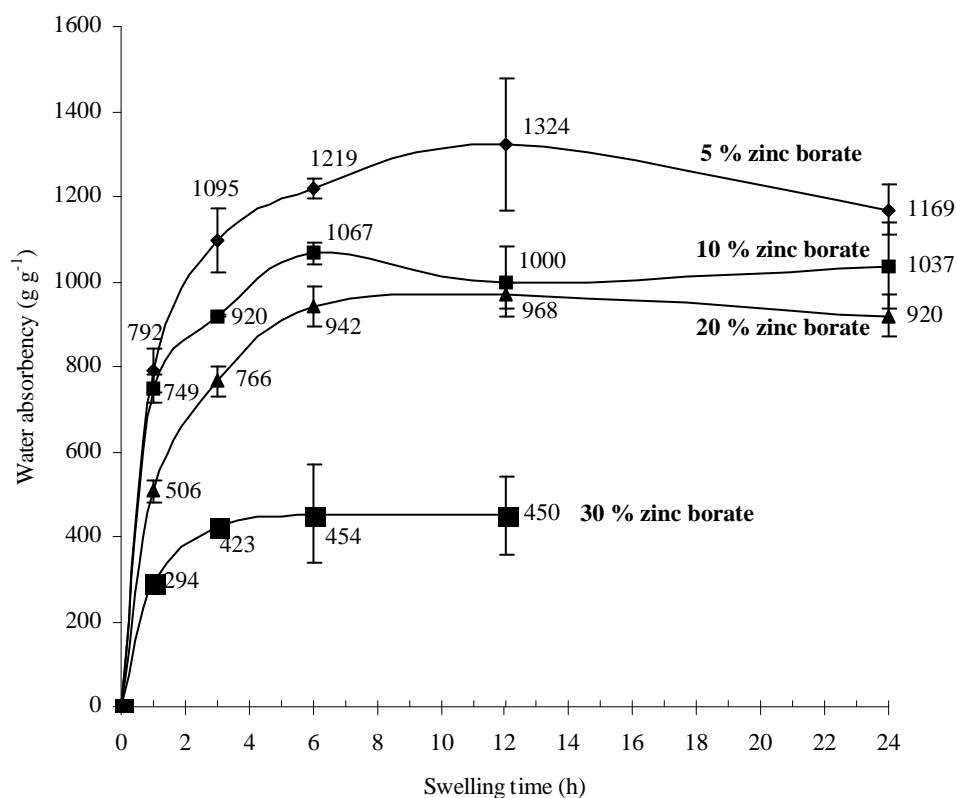
Figure 4.16 Deionized water absorbency of zinc borate incorporated SAPC at various swelling times

4.5.3 Swelling kinetic of poly(AM-*co*-AMPS-Na+)/melamine nano-composites

The deionized water absorbency of the melamine incorporated SAPCs at various swelling times is shown in Figure 4.17. Unlike the 30% w w^{-1} melamine incorporated SAPCs, the same amount of melamine added into the reaction mixture yielded a homogeneous system. The addition of melamine decreased water

absorbency of the melamine incorporated SAPCs. It is supposed that hydrogen bonding between the N atoms in melamine with the carbonyl group of acrylamide or sulfonate group of AMPS-Na$^+$ may contribute to the physical stability and the lower water absorption capacity of the composite SAPCs.
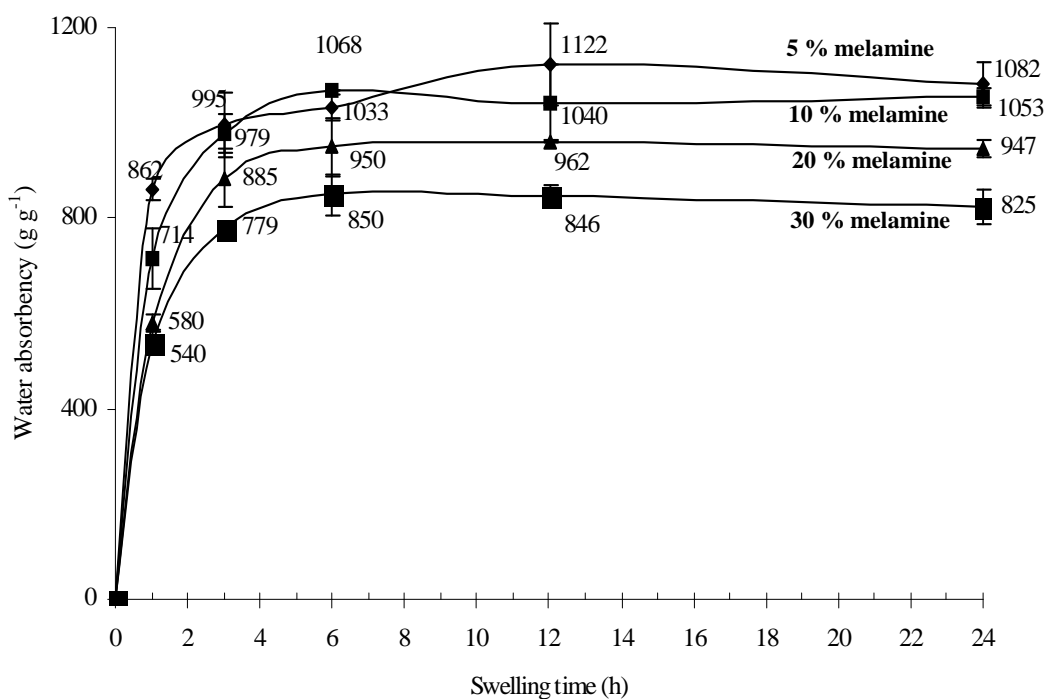
Figure 4.17 Deionized water absorbency of melamine incorporated SAPs at various swelling time**s**

4.6 Effect of tap water absorbency of the superabsorbent nanocomposites

Tap water absorbency of SAPCs is shown in Figures 4.18 - 4.20.
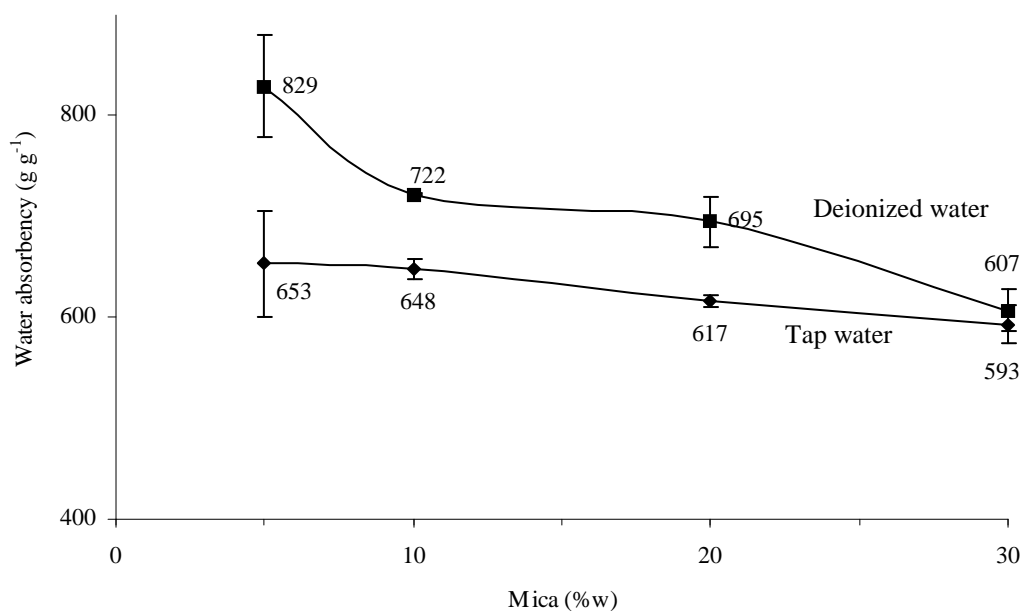
Figure 4.18 water absorbency of mica incorporated SAP in deionized water and tap water
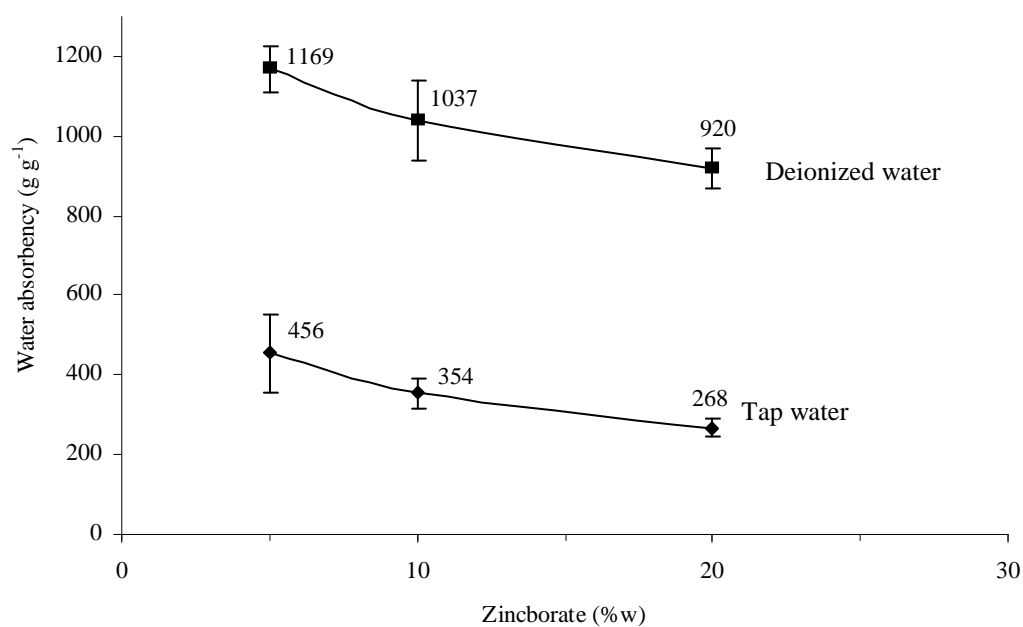
Figure 4.19 Water absorbency of zinc borate incorporated SAPC in deionized water and tap water
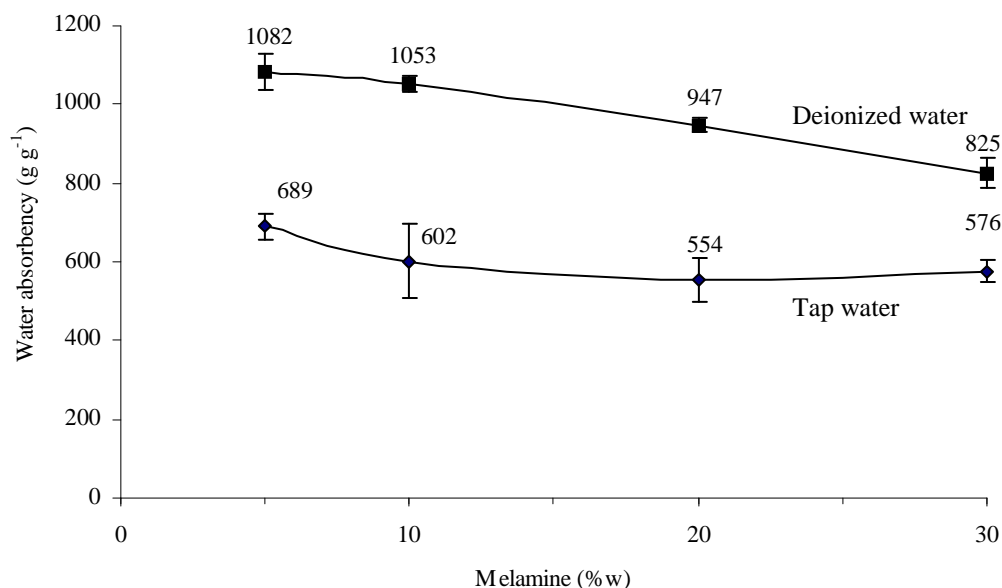
Figure 4.20 Water absorbency of melamine incorporated SAPC in deionized water and tap water

Water absorbency in tap water of the three SAPCs as shown in Figures 4.18 - 4.20 is always lower than those in the deionized water. The difference in water absorption is caused by the presence of different ions. The tap water used here contains Fe^{3+} (7.2 ppm), Ca^{2+} (27.2 ppm) and Mg^{2+} (0.05 ppm) as the dominate ions. The main reason is the shielding or screening effects of the cations that reduces osmotic pressure of the systems. Comparing the effect of the ions on the three SAPCs, one can see that the zinc borate incorporated SAPCs were affected most because the water absorption was reduced most. One possible cause can be the synergistic effect of Zn^{2+}, and the three multivalent cations of Fe^{3+}, Ca^{2+} and Mg^{2+}. For the SAPC incorporating either melamine or mica, the effect of the cations with melamine or mica is not so strong due to the less polarity of melamine or less interaction between complex ions in mica and the mentioned mentioned cations in tap water.

Effect of major ions on SAPs/melamine and SAPs/mica parts were decreased insignificantly because low polarity of melamine and mica supports the divalent and trivalent cations in tap water.

4.7   Thermal properties of the superabsorbent nanocomposites

4.7.1 Thermal properties of mica and poly(AM-*co*-AMPS-Na$^+$)/mica superabsorbent nanocomposites

Thermal stability of pristine mica and poly(AM-*co*-AMPS-Na$^+$)/mica nanocomposites was evaluated using TGA and their thermograms are shown in Figure 4.21. Table 4.10 elucidates the data extracted from Figure 4.21. Pristine mica has one degradation stage, which was moisture containing of mica in the range of 68 – 87 °C with a weight loss of 7.3% (Figure 4.21 (a)). The DTG maxima of poly(AM-*co*-AMPS-Na$^+$)/mica nanocomposites at mica loadings of 5, 10, 20 and 30 %w w^{-1} are similar to the thermal decomposition of poly(AM-*co*-AMPS-Na$^+$) superabsorbents. The first stage of degradation temperature of all nanocomposites takes place in the range of 40 – 125 °C corresponding to the absorbed and bound water with a weight loss of 13.2 – 15.1%. The second stage in the range of 307 – 329 °C is ascribed to the amide side group of the AMPS-Na$^+$ having a weight loss of 14.9 – 21.8%. The third stage in the range of 329 – 413 °C is interpreted as the amide side group of AM and the physical crosslink with mica having a weight loss of 13.6 – 16.6%. The final stage in the range of 450 – 800 °C is assigned to the degradation of chain backbone with a weight loss of 11.3 – 18.9% (Zhang and Wang, 2007).
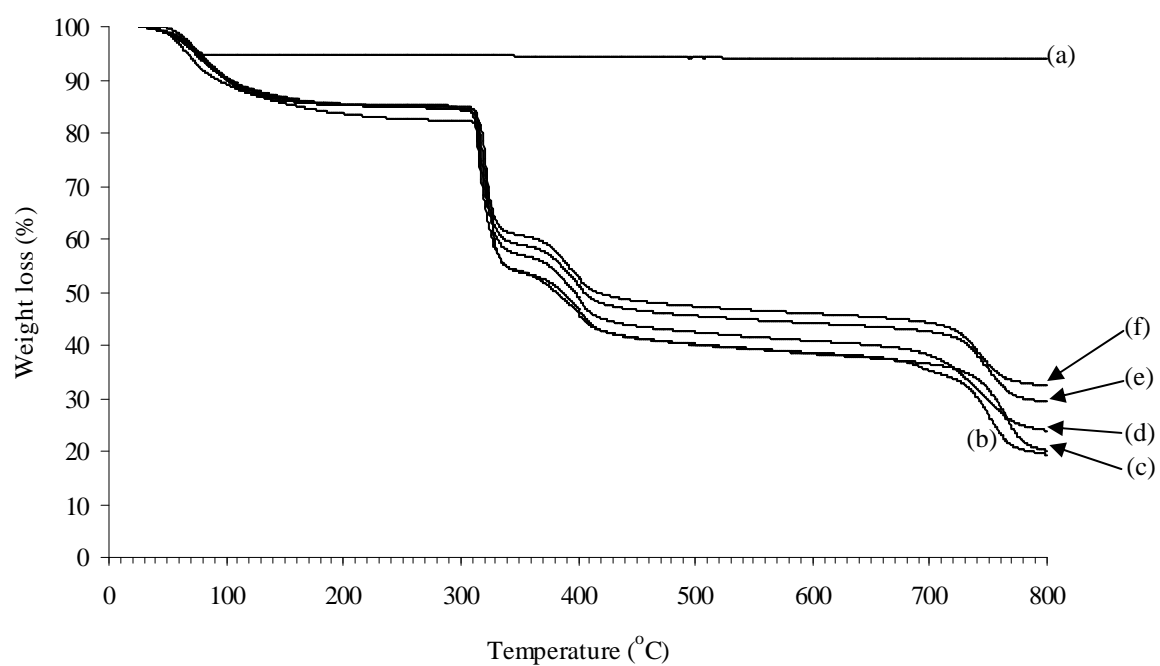
Figure 4.21 All TGA thermograms of (a) mica, (b) poly(AM-*co*-AMPS-Na$^+$) superabsorbents, and (c-f) for poly(AM-*co*-AMPS-Na$^+$)/mica nanocomposites at 5, 10, 20, and 30% w w^{-1} of mica, respectively.

Table 4.10 Thermogravimetry of poly(AM-*co*-AMPS-Na$^+$)/mica nanocomposites

Mica loading (%w w^{-1} of all monomers)	Number of decomposition stage	Temperature range (°C)	DTG maxima (˚C)**	Weight loss (%)	Residue at 800 °C
Pure mica	1	68-87	73	7.3	92.6
	2	351-402	378	0.2	
0	1	40-121	68	15.1	19.4
	2	316-329	322	19.6	
	3	329-413	331	16.6	
	4	718-800	752	14.4	
5	1	42-125	70	13.4	20.1
	2	316-327	323	14.5	
	3	327-413	330	16.5	
	4	719-800	768	15.6	
10	1	42-125	75	13.2	23.9
	2	316-327	316	21.6	
	3	327-413	402	14.2	
	4	719-800	748	13.1	
20	1	42-125	82	14.6	29.3
	2	308-327	317	20.6	
	3	327-409	403	13.6	
	4	714-800	768	12.6	
30	1	42-125	81	13.8	32.3
	2	307-327	318	18.9	
	3	327-407	404	13.8	
	4	709-800	739	11.5	

**DTG is differential thermal gravimetry.

The thermal stability and the residues at 800 °C of the nanocomposites increased in relation to the amount of mica present in the system. This improvement of thermal stability characteristic in the composites could be attributed to the pronounced thermal stability of mica and to the interaction between the mica particles and the polymer matrix (Chang *et al*., 2003). Regardless of the mica content loaded,

the calculated amount of residues at 800 ^{o}C from the thermograms revealed that approximately 70% w w^{-1} of the mica was retained in the superabsorbent nanocomposites. The rest of mica (30%) was not employed in the synthesis reactions and might be removed during the precipitation process.

The TGA results shown in Table 4.10 confirm that mica indeed improved thermal stability of the superabsorbent nanocomposites at all temperature ranges because mica acts as a heat barrier to delay the diffusion of volatile thermo-oxidation products to gas, and gas from the nanocomposite (Zhang *et al.,* 2007). Thereby, thermal stability of poly(AM-*co*-AMPS-Na^{+})/mica superabsorbent nanocomposites increased with increasing mica loadings.

4.7.2 Thermal properties of poly(AM-*co*-AMPS-Na^{+})/zinc borate superabsorbent nanocomposites

Thermal behavior of zinc borate superabsorbent nanocomposites is revealed via TGA thermographs as shown in Figure 4.22 and Table 4.11. The DTG maxima of poly(AM-*co*-AMPS-Na^{+})/zinc borate superabsorbent composites at the zinc borate loadings of 5, 10, 20 and 30 %w w^{-1} have a similar profile with the thermal decomposition of poly(AM-*co*-AMPS-Na^{+}) superabsorbents. The first stage of degradation temperature of all superabsorbents takes place in the range of 48 – 103 °C corresponding to the absorbed and bound water with a weight loss of 6.1 – 9.0%. The second stage in the range of 313 – 328° C is ascribed to the amide side group of the AMPS-Na^{+} having a weight loss of 19.2 – 21.4%. The third stage in the range of 325 – 433 °C is interpreted as the decomposition of the amide side group of AM (Zhang and Wang, 2007) and the dehydration of zinc borate crystal with a weight loss of 12.4 − 21.3%. The pure zinc borate has an important degradation stage, which is the dehydration of zinc borate crystal in the temperature range of 341 – 416 °C with a

weight loss of 11.2%. The final stage in the range of 711 – 800 °C is assigned to the degradation of chain backbone and rearranged zinc borate (Genovese and Shanks, 2007) with a weight loss of 10.7 – 15.1%.
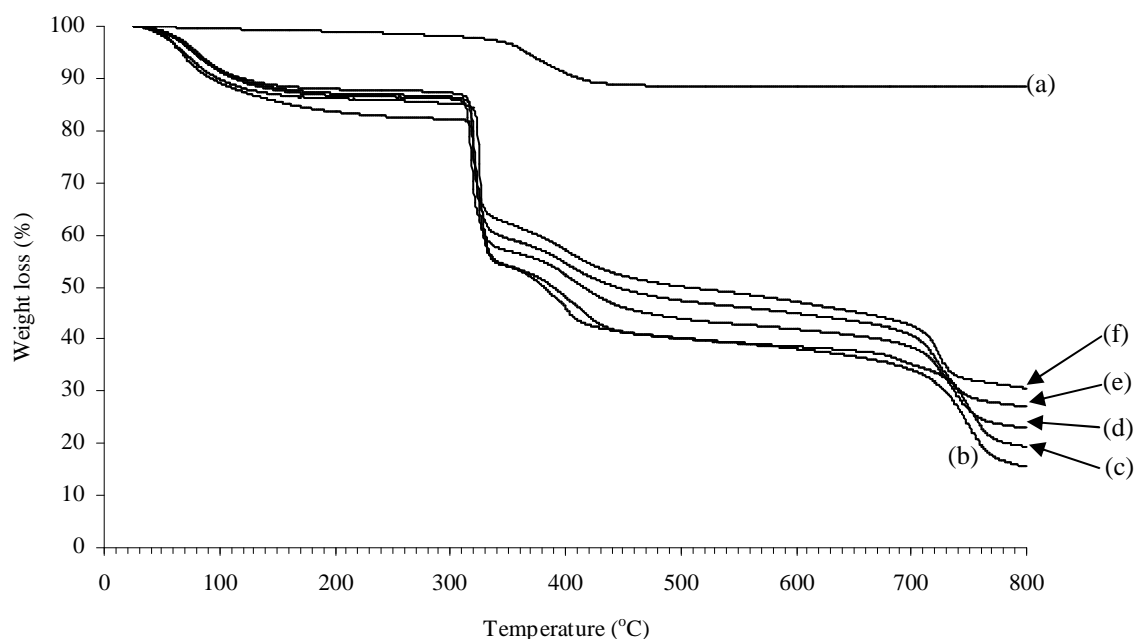
Figure 4.22 All TGA thermograms of (a) zinc borate, (b) poly(AM-*co*-AMPS-Na$^+$) superabsorbents, and (c-f) for poly(AM-*co*-AMPS-Na$^+$)/zinc borate nanocomposites at 5, 10, 20, and 30 % w w^{-1} of zinc borate, respectively.

The results indicated that zinc borate enhanced thermal stability of the prepared superabsorbent nanocomposites at all temperatures. Beyond 320 °C, such a modification in thermal stability was obviously detected as a function of zinc borate loading because zinc borate can rearrange its structure and therefore acts as a heat barrier to delay the diffusion of volatile thermo-oxidation products to gas, and gas to the composite (Genovese and Shanks, 2007). Thermal stability of poly(AM-*co*-AMPS-Na$^+$)/zinc borate nanocomposite superabsorbents increases with increasing zinc borate loadings.

Table 4.11 Thermogravimetry of poly(AM-*co*-AMPS-Na$^+$)/zinc borate superabsorbent nanocomposites

Zinc borate loading (%w w^{-1} of totals monomer)	Number of decomposition stage	Temperature range (°C)	DTG maxima (°C)	Weight loss (%)	Residue at 800°C
Pure zinc borate	1	341-416	379	11.2	86.7
0	1	40-121	68	15.1	19.4
	2	316-329	322	19.6	
	3	329-413	331	16.6	
	4	718-800	752	14.4	
5	1	48-102	71	9.0	15.5
	2	319-328	326	20.3	
	3	328-430	330	21.3	
	4	727-800	748	15.1	
10	1	58-101	82	7.0	22.9
	2	315-325	318	19.2	
	3	325-431	331	15.7	
	4	714-800	734	13.8	
20	1	61-103	8	6.8	27.0
	2	314-328	322	21.4	
	3	328-433	332	13.5	
	4	711-800	723	12.1	
30	1	60-102	76	6.1	30.5
	2	313-328	321	20.7	
	3	328-433	332	12.4	
	4	711-800	724	10.7	

4.7.3 Thermal properties of poly(AM-*co*-AMPS-Na$^+$)/melamine superabsorbent nanocomposites

Figure 4.23 and Table 4.12 show TGA thermograms and the data extracted from the thermograms, respectively. Pure melamine shows two degradation stages from which nitrogen volatile side groups were generated in the first stage. The

second stage was the decomposition of main chain and nitrogen volatiles from the first stage (Liang *et al*., 2004). The DTG maxima of poly(AM-*co*-AMPS-Na$^+$)/ melamine superabsorbent nanocomposites at the melamine loadings of 5, 10, 20 and 30 %w w^{-1} have a similar profile to the thermal decomposition of poly(AM-*co*-AMPS-Na$^+$) superabsorbents. The first stage of degradation temperature of all superabsorbents takes place in the range of 33 – 161 °C corresponding to the absorbed and bound water with a weight loss of 6.0 – 15.1%. The second stage in the range of 282 – 310°C is ascribed to the decomposition of the N$_2$ gas from melamine having a weight loss of 5.9 – 7.4%. The third stage in the range of 313 –346 °C is interpreted for the AMPS-Na$^+$ with a weight loss of 31.0 – 32.8%. The fourth stage in the range of 345 – 412 °C is interpreted as the decomposition of the AM with a weight loss of 31.0 – 32.8% .The final stage in the range of 742 – 800°C is assigned to the degradation of chain backbone with a weight loss of 11.1 – 12.2%.
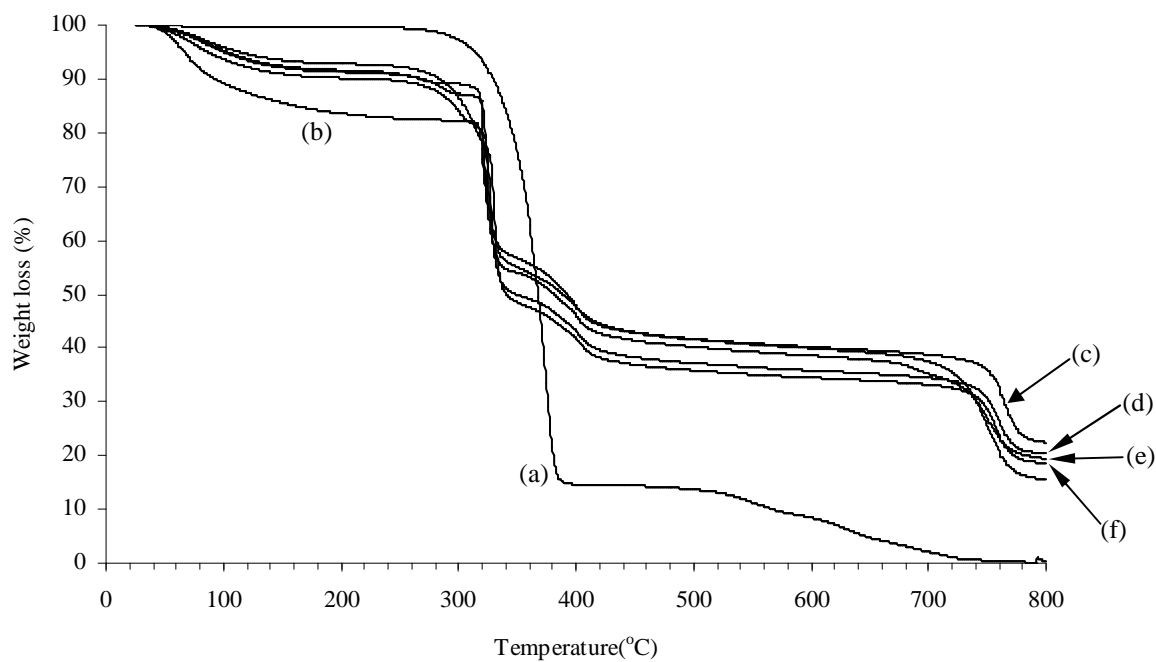
Figure 4.23 All TGA thermograms of (a) melamine, (b) poly(AM-*co*-AMPS-Na$^+$)

superabsorbents, and (c-f) for poly(AM-*co*-AMPS-Na$^+$)/melamine nanocomposites at

5, 10, 20, and 30% w w^{-1} of melamine, respectively.

Table 4.12 Thermogravimetry of poly(AM-*co*-AMPS-Na$^+$)/melamine superabsorbent nanocomposites

Melamine loading (%w w^{-1} of totals monomer)	Number of decomposition stage	Temperature range (°C)	DTG maxima (˚C)	Weight loss (%)	Residue at 800°C
Pure melamine	1	315-381	351	87.3	0.1
	2	416-748	643	12.6	
0	1	40-161	68	15.1	19.4
	2	316-329	322	19.6	
	3	329-413	331	16.6	
	4	718-800	752	14.4	
5	1	43-135	83	6.9	15.5
	2	318-341	323	29.7	
	3	341-411	402	12.4	
	4	738-800	749	15.5	
10	1	45-145	85	7.3	22.5
	2	320-342	325	36.3	
	3	342-411	402	10.3	
	4	748-800	767	13.7	
20	1	33-133	72	8.4	20.3
	2	282-310	303	5.9	
	3	314-345	328	31.0	
	4	345-412	406	9.9	
	5	747-800	706	11.1	
30	1	34-134	82.5	6.0	18.5
	2	282-310	310	7.4	
	3	313-346	332	32.8	
	4	346-412	406	9.8	
	5	742-800	757	12.2	

It was found that incorporation of melamine improved the thermal stability of the SAPC until 300 °C because melamine generates N_2 gas in these temperature ranges. The N_2 gas dilutes the O_2 gas and covers the SAPC surface. The thermal stability of poly(AM-*co*-AMPS-Na$^+$)/melamine nanocomposite superabsorbents thus increases with increasing melamine loadings.

4.8 Effect of the incorporation of combined zinc borate and melamine on water absorbency and thermal property of the superabsorbent nanocomposites

4.8.1 Water absorbency

The equilibrium water absorbency of the poly(AM-*co*-AMPS-Na$^+$)/zinc borate/melamine superabsorbent nanocomposites synthesized with various mica loadings is shown in Table 4.13 and Figure 4.24.

Table 4.13 Effect of zinc borate-to-melamine ratios on equilibrium water absorbency poly(AM-*co*-AMPS-Na$^+$)/zinc borate/melamine superabsorbent nanocomposites

zinc borate-to-melamine ratios (% w w^{-1} of total monomers)	Equilibrium water absorbency (g g^{-1})
30:0	N/A
20:10	668±8
15:15	699±4
10:20	723±34
0:30	825±37

The results are the average in triplicate; N/A = the product appeared as heterogeneous phase.
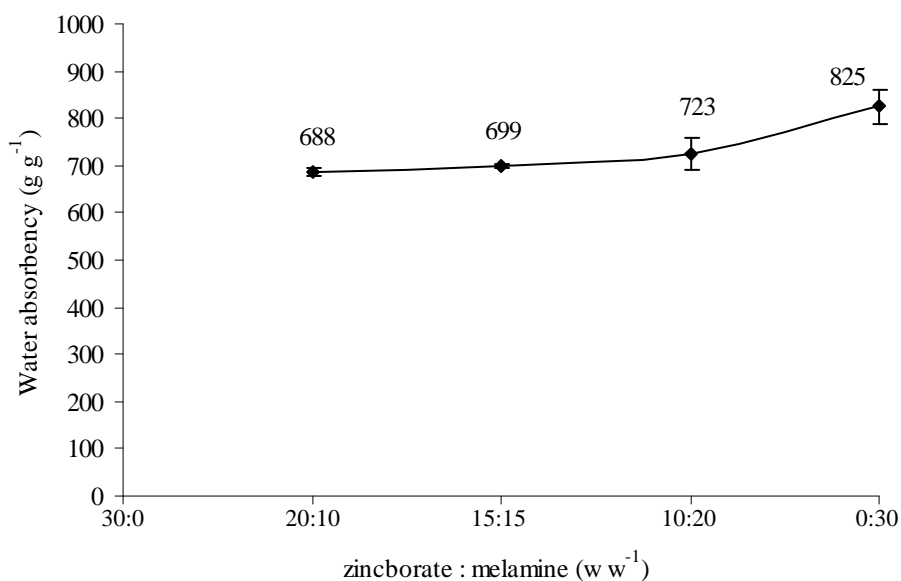
Figure 4.24 Effect zinc borate-to-melamine ratios on the equilibrium water absorbency of poly(AM-*co*-AMPS-Na$^+$)/zinc borate/melamine superabsorbent nanocomposites with various zinc borate-to-melamine ratios at: 30:0, 20:10, 15:15, 10:20 and 0:30% w w^{-1} of total monomers (All superabsorbent nanocomposites are prepared with AM-to-AMPS-Na$^+$ molar ratio at 15 : 85, 0.05% mol N-MBA,0.6% APS, 0.6% TEMED and 10 ml of reaction medium)

Table 4.13 and Figure 4.24 show the equilibrium water absorbency of poly(AM-*co*-AMPS-Na$^+$)/zinc borate /melamine nanocomposite superabsorbents. The zinc borate-to-melamine ratios at 20:10 %w w^{-1}, equilibrium water absorbency decreases markedly by 43% compared with poly(AM-*co*-AMPS-Na$^+$) superabsorbents. Furthermore, when the zinc borate-to-melamine ratios were 15:15, 10:20 and 0: 30 %w w^{-1}, the equilibrium water absorbency was slightly increased compared with zinc borate-to-melamine ratios at 20: 10% w w^{-1}. This is because the polarity of the SAPs increases with increasing the content of melamine.

4.8.2 Thermal property

Table 4.14 shows the thermogravimetry of poly(AM-*co*-AMPS-Na$^+$)/zinc borate/melamine superabsorbent nanocomposites.

Table 4.14 Thermogravimetry of poly(AM-*co*-AMPS-Na$^+$)/zinc borate/melamine superabsorbent nanocomposites

zinc borate-to-melamine ratios (%w w^{-1} of totals monomer)	Number of decomposition stage	Temperature range (°C)	DTG maxima (°C)	Weight loss (%)	Residue at 800°C
30:0	1	60-102	76	6.1	
	2	313-328	321	20.7	30.5
	3	328-433	332	12.4	
	4	711-800	724	10.7	
20:10	1	42-107	85	9.1	
	2	331-342	329	16.6	26.3
	3	342-419	347	7.5	
	4	727-800	761	7.3	
15:15	1	42-108	83	9.5	
	2	334-346	331	17.0	23.3
	3	346-419	349	6.5	
	4	727-800	762	8.3	
10:20	1	42-108	83	9.3	
	2	330-343	328	24.2	20.8
	3	343-419	348	7.9	
	4	727-800	761	10.0	
0:30	1	34-134	82.5	6.0	
	2	282-310	310	7.4	
	3	313-346	332	32.8	18.5
	4	346-412	406	9.8	
	5	742-800	757	12.2	

From Table 4.14 and Figures 4.24 (a−e), the DTG maxima of poly(AM-*co*-AMPS-Na$^+$)/melamine/zinc borate superabsorbent nanocomposites at zinc borate-to-melamine ratios of 20 : 0, 20 : 10, 15 : 15, 10 : 20 and 0 : 30% w w^{-1} of total monomers are similar to the thermal decomposition of poly(AM-*co*-AMPS-Na$^+$)/melamine and poly(AM-*co*-AMPS-Na$^+$)/zinc borate superabsorbent nanocomposites. The first stage of degradation temperature of all nanocomposites takes place in the range of 42−108 °C corresponding to the absorbed and bound water with a weight loss of 9.1−9.3%. The second stage in the range of 330–346 °C is ascribed to depolymerization and/or decomposition of the N$_2$ from melamine and decomposition of the AMPS-Na$^+$ having a weight loss of 16.6−24.2%. The third stage in the range of 342–419 °C is interpreted as the decomposition of acrylamide and rearrangement of zinc borate with a weight loss of 6.5 - 7.9%. The final stage in the range of 727–800 °C is assigned to the degradation of poly(AM-*co*- AMPS-Na$^+$) with a weight loss of 20.8–26.3 %.

From Figure 4.25 was found that has 2 temperature ranges to observation. In the first range (25–341 °C), thermal stability was found to increase with increasing melamine ratio but decrease with increasing zinc borate ratio and the second range (above 341 °C), thermal stability was found to increase with increasing zinc borate ratio but decrease with increasing melamine ratio.

Appropriate zinc borate-to-melamine ratio depended on specific work, which was considered from the desired water absorbency and the operated temperature range for fire retardation.
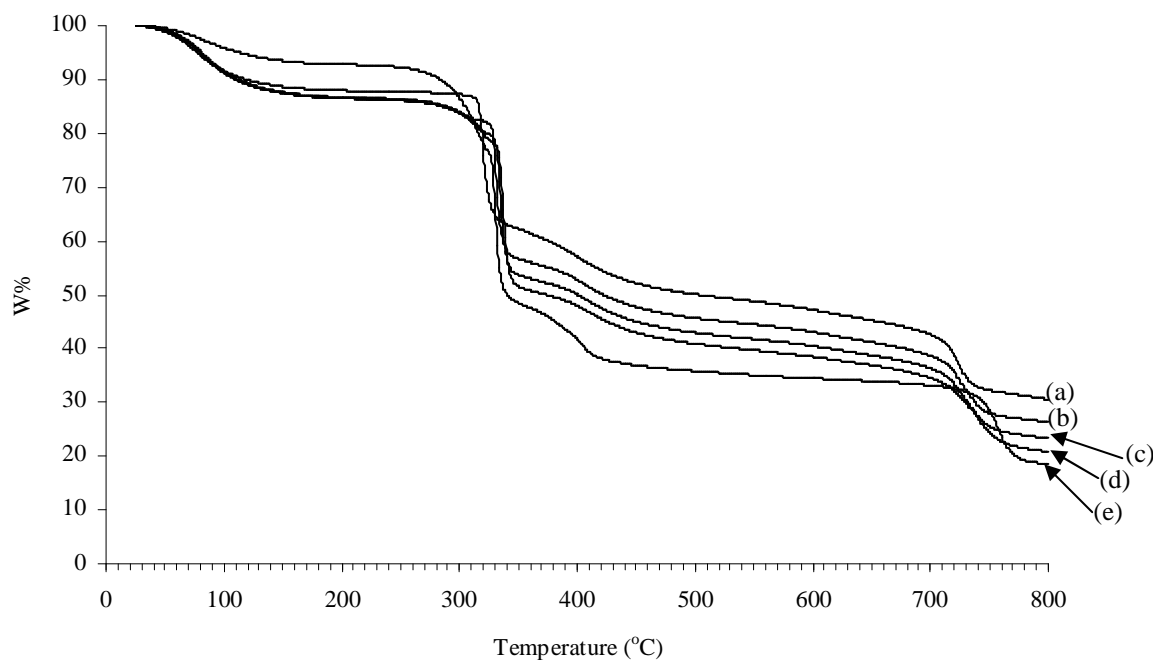
Figure 4.25 All TGA thermograms of poly(AM-*co*-AMPS-Na$^+$)/zinc borate/melamine nanocomposite superabsorbents with various zinc borate-to-melamine ratios at (a) 30 : 0, (b) 20 : 10, (c) 15 : 15, (d) 10 : 20 and (e) 0 : 30 %w w^{-1} of total monomers

4.9   Flammability testing

A flammability characterization was carried out using a cone calorimeter at an incident heat flux of 50 kW m^{-2}, in air atmosphere, and the flame temperature was 885°C. After being directly exposed to the flame, the times to ignition of the specimens with different types of gel coating were recorded as shown in Table 4.15. An uncoated wood board, a control specimen, was exposed to the flame and burst to become red flame within approximately 13 s. However, all the gel gave excellent protection to the wood. The wood specimens coated with SAPs-coating, SAPs/20% zinc borate-coating, and SAPs/30% melamine-coating were ignited within a similar duration time (about 120-140 s). The SAPs/30% mica- coated wood specimen and

SAPs/20% zinc borate/10% melamine-coated wood specimen gave a longer duration time to ignition at 186 and 258 s, respectively. The results therefore showed that all SAP coated wood specimens delayed the ignition time after being exposed to an open flame in comparison with the uncoated wood specimen.

When comparing the type of coating SAP, the total time for the flame to penetrate through the SAP coating layer was found to vary among the samples. The result suggested that all SAP composites provided the longer duration times to burn all the coated gels ranging from 60-120 s, whereas the time to burn down the SAPs-coated layer was only 4 s after the ignition. This was attributed by the presence of mica as a thermal barrier in the SAPs/30% mica-coated surface, which retarded diffusion of heat and slowed down the burning. Likewise, the duration for char formation and its appearance in the coated specimens with SAPs containing zinc borate and/or melamine indicates that the SAPCs or SAP filled with fire retardant act as a heat barrier to prolong the heat migration resulting in the lower burning rate. The in-depth mechanism of the fire retardants or mica is under investigation.

Table 4.15 Time to ignition, time to burn of all the coated SAPCs on wood specimens and color of the chars

Specimen	Time to ignition (s)	Time to burn (s)	Color of the char
Uncoated wood	13	-	Dark gray
SAPs coated on wood	136	4	White
SAPs/30% mica coated on wood	186	84	Black
SAPs/20% zinc borate coated on wood	118	96	White and yellow
SAPs/30% melamine coated on wood	117	119	Gray
SAPs/20% zinc borate/10% melamine coated on wood	258	60	White and gray

Charred samples after flammability test are shown in Figure 4.26. In Figure 4.26(a), the uncoated wood gave the dark gray char. Figure 4.2.6(b) – (f) illustrate that the chars of the wood boards coated with SAPs are white, SAPs/30% mica are black lump char. The burning of SAPs/20% zinc borate generated white and yellow char, SAPs/30% melamine gave gray char, and SAPs/20% zinc borate/10% melamine produced white and gray char.

(a)
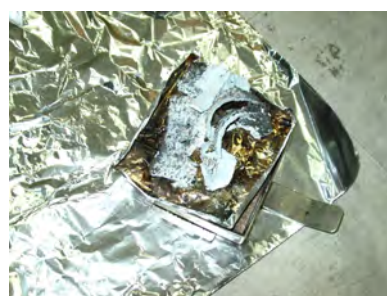
(b)
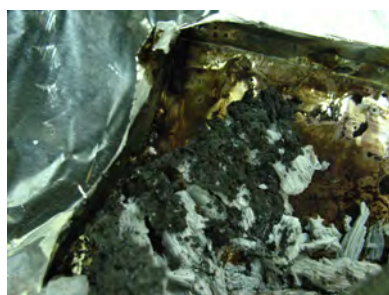
(c)

(d)

(e)

(f)

Figure 4.26 Charred samples of (a) uncoated wood board, and the wood board coated with (b) SAPs, (c) SAPs/30% mica, (d) SAPs/20% zinc borate, (e) SAPs/30% melamine and (f) SAPs/20% zinc borate/10% melamine

CHAPTER V

CONCLUSIONS AND SUGGESTIONS

5.1 Conclusions

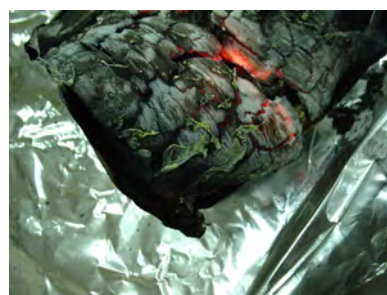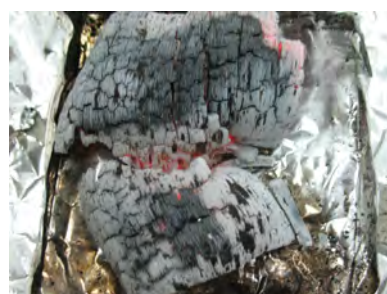Poly(AM-*co*-AMPS-H$^+$), poly(AM-*co*-AMPS-Na$^+$) and all composites of poly(AM-*co*-AMPS-Na$^+$)/fire retardants were synthesized and characterized by FTIR spectroscopy, TEM, TGA, XRD and equilibrium water absorbency. The FTIR spectrum of all poly(AM-*co*-AMPS-Na$^+$)/fire retardants showed the characteristic peaks of poly(AM-*co*-AMPS-Na$^+$) moiety and all fire retardants. This confirmed the presence of poly(AM-*co*-AMPS-Na$^+$)/fire retardant superabsorbent nanocomposites.

The equilibrium water absorbency of poly(AM-*co*-AMPS-Na$^+$) increased with increasing ionic monomer contents. When N-MBA and APS content increased, the equilibrium water absorbency decreased whereas TEMED content slightly increased the water absorbency of poly(AM-*co*-AMPS-Na$^+$). The water absorbency reached equilibrium point at 6 h in tap water caused decreasing water absorbency of all superabsorbent nanocomposites.

The intercalation was confirmed by XRD pattern and TEM micrographs. The poly(AM-*co*-AMPS-Na$^+$)/mica superabsorbent nanocomposites had better thermal stability than the neat superabsorbent polymer, swollen gel strength but decreased water absorbency of superabsorbent nanocomposites.

Thermal stability was proven by TGA and cone calorimetric technique. The poly(AM-*co*-AMPS-Na$^+$)/fire retardants exhibited the improved thermal stability with increasing leading loadings of the fire retardants.

5.2 Suggestions for future work

To complete the part of poly(AM-*co*-AMPS-H$^+$), water absorbency of all molar ratios should be investigated. The chemical structure for MHAB part should be analyzed. Fire retardant additives should be confirmed by EDXS technique.

REFERENCES

Adhikari, B. and Majumdar, S. (2004). Polymers in sensor applications. *Progress in Polymer Science* 29: 699–766.

Bordado J. C. M. and Gomes, J. F. P. (2007). New technologies for effective forest fire fighting. *International Journal of Environmental Studies* 64: 243 – 251.

Bozhilov, K. N., Xu, Z., Dobrzhinetskaya, L. F., Jin, Z. M. and Green II, H. W. (2009). Cation-deficient phlogopitic mica exsolution in diopside from garnet peridotite in SuLu, China. *Lithos* 109: 304-313.

Braun, U., Schartel, B., Fichera, M. A. and Jager, C. (2007). Flame retardancy mechanisms of aluminium phosphinate in combination with melamine polyphosphate and zinc borate in glass-fibre reinforced polyamide 6,6. *Polymer Degradation and Stability* 92: 1528-1545.

Buchholz F. L. and Burgert J.H. (1996). Synthesis and applications of superabsorbent polymers in *Industrial water soluble polymers*, Finch, C.A. (Ed.), Royal Society of Chemistry, Cambridge, p. 93.

Cai, Y., Wei, Q., Huang, F. and Gao, W. (2008). Preparation and properties studies of halogen-free flame retardant form-stable phase change materials based on paraffin/high density polyethylene composites. *Applied Energy* 85: 765–775.

Chang, J. H., An, Y. U., Cho, D. and Giannelis E. P. (2003). Poly(lactic acid) nanocomposites: comparison of their properties with montmorillonite and synthetic mica (II). *Polymer* 44: 3715–3720.

Chen, R., Peng, F. and Su, S. (2008). Synthesis and characterization of novel swelling tunable oligomeric poly(styrene-co-acrylamide) modified clays. *Journal of Applied Polymer Science* 108: 2712–2717.

Chen, L. and Wang Y. Z. (2009). A review on flame retardant technology in China. Part I: development of flame retardants. *Polymers for Advanced Technologies* 21: 1-26.

Dai, H., Li, H. and Wang, F. (2006). An alternative process for the preparation of Cu-coated mica composite powder. *Surface & Coatings Technology* 201: 2859–2866.

Foungfunga, D., Phattanarudeeb, S., Seetapanc, N. and Kiatkamjornwong, S. (2009). Acrylamide–itaconic acid superabsorbent polymers and superabsorbent polymer/mica nanocomposites. *Polymers for Advanced Technologies*, DOI: 10.1002/pat. 1559.

Durmaz, S. and Okay, O. (2000). Acrylamide/2-acrylamido-2-methylpropane sulfonic acid sodium salt-based hydrogels: synthesis and characterization. *Polymer* 41: 3693–3704.

Elliott, M. (2004). Product Development scientist for SAP. BASF Aktiengsell schaft.

El-Rehim, H. A., Hegazy, E. A. and El-Mohdy, H. A. (2006). Effect of various environmental conditions on the swelling property of PAAm/PAAcK superabsorbent hydrogel prepared by ionizing radiation. *Journal Applied Polymer Science* 101: 3955–3962.

Folaranmi, J. (2009). Effect of additives on the thermal conductivity of clay. *Leonardo Journal of Sciences* 14: 74-77.

Garcia-Gonziilez, N., Kellaway, I.W., Blanco-Fuente, H., Anguiano-Igea, S., Delgado-Charro, B., Otero-Espinar, F.J. and Blanco-MCndez, J. (1993). Design and evaluation of buccoadhesive metoclopramide hydrogels composed of poly(acrylic acid) crosslinked with sucrose. *International Journal of Pharmaceutics* 100: 65-70.

Genovese, A. and Shanks, R. A. (2007). Structural and thermal interpretation of the synergy and interactions between the fire retardants magnesium hydroxide and zinc borate. *Polymer Degradation and Stability* 92: 2-13.

Guilherme, M.R., Reis, A.V., Paulino, A.T., Fajardo, A.R., Muniz, E.C. and Tambourgi, E.B. (2007). Superabsorbent hydrogel based on modified polysaccharide for removal of Pb^{2+} and Cu^{2+} from water with excellent performance. *Journal of Applied Polymer Science* 105: 2903–2909.

Hu, Y., Ye, L. and Zhao, X. (2006). Synthesis of the melamine–formaldehyde polycondensate and its thermal stabilization effect on polyoxymethylene. *Polymer* 47: 2649–2659.

Ibrahim, S.M., El-Salmawi, K.M. and Zahran, A.H. (2007). Synthesis of crosslinked superabsorbent carboxymethylcellulose/acrylamide hydrogels through electron-beam irradiation. *Journal of Applied Polymer Science* 104: 2003–2008.

Innes, J. D. (1996). Flame retardants and their market applications. *Fire Retardant Chemicals Association*, Baltimore: 61–69.

Jiang, F., Li, W., Zhan, X., Chen, G., Zhou, J., Huang, J. and Zhang, S. (2006). Preparation and charcterization of konjac superabsorbent polymer. *Journal of Wuhan University of Technology* 21: 87-91.

Kiatkamjornwong, S., Chomsaksakul, W. and Sonsuk, M. (2000). Radiation modification of water absorption of cassava starch by acrylic acid/acrylamide. *Radiation Physics and Chemistry* 59: 413-427.

Kiatkamjornwong, S. (2007). Superabsorbent polymers and superabsorbent polymer composites. *ScienceAsia* 33: 39-43.

Kim, J., Lee, K., Hefferan, T., Currier, B., Yaszemski, M. and Lu, L. (2008). Synthesis and evaluation of novel biodegradable hydrogels based on poly(ethylene glycol) and sebacic acid as tissue engineering scaffolds. *Biomacromolecules* 9: 149–157.

Koytepe, S., Vural S. and Seckin, T. (2009). Molecular design of nanometric zinc borate-containing polyimide as a route to flame retardant materials. *Materials Research Bulletin* 44: 369-376.

Li, J. J., Huang, X. B. and Cai, T.M. (2003). Flame-retarded styrene plastics. *Science Press*, Beijing

Liang, H., Asif, A. and Shi, W. (2005). Thermal degradation and flame retardancy of a novel methacrylated phenolic melamine used for UV curable flame retardant coatings. *Polymer Degradation and Stability* 87: 495-501.

Lin, S. B., Yuan, C. H., Ke, A. R. and Quan, Z. L. (2008). Electrical response characterization of PVA–P(AA/AMPS) IPN hydrogels in aqueous Na_2SO_4 solution. *Sensors and Actuators B* 134: 281–286.

Liu, Y., Wang, J. S., Deng, C. L., Wang, D. Y., Song Y. P. and Wang, Y. Z. (2009). The synergistic flame-retardant effect of O-MMT on the intumescent flame-retardant PP/CA/APP systems *Polymers for Advanced Technologies*, DOI 10.1002/pat.1502.

Lu, H., Hu, Y., Li, M. and Song, L. (2008). Clay intercalation and influence on flammability and crystallization behaviors of POE-based nanocomposites. *Polymer Composites*: 29: 1358-1363.

Marandi, G. B., Esfandiari, K., Biranvand, F.,Babapour, M., Sadeh, S. and Mahdavinia, G. R. (2008). pH sensitivity and swelling behavior of partially hydrolyzedformaldehyde-crosslinked poly(acrylamide) superabsorbent hydrogels. *Journal Applied Polymer Science* 109:1083–1092.

Ma, Z., Zhao, W., Liu, Y. and Shi, J. (1998). Synthesis and properties of intumescent, phosphorus-containing, flame-retardant polyesters. *Journal of Applied Polymer Science* 63: 1511-1515.

Murthy, P.S.K., Mohan, Y.M., Varaprasad, K., Sreedhar, B. and Raju, K.M. (2008). First successful design of semi-IPN hydrogel–silver nanocomposites: a facile approach for antibacterial application. *Journal of Colloid and Interface Science* 318: 217–224.

Nachash, H. J. and Okay, O. (1996). Formation and structure of polyacrylamide gels. *Journal of Applied Polymer Science* 60: 971-979.

Nalampang, K., Suebsanit, N., Witthayaprapakorn, C., and Molloy, R. (2007). Design and Preparation of AMPS-based hydrogels for biomedical use as wound dressings. *Chiang Mai Journal Science* 34: 183-189.

Nazare S., Kandola B. K. and Horrocks A. R. (2008). Smoke, CO, and CO_2 measurements and evaluation using different fire testing techniques for flame retardant unsaturatedpolyester resin formulations. *Journal of Fire Sciences* 26: 215–242.

Odian, G. Principles of Polymerization, Fourth Edition, Wiley & Son, New York, p. 244-245.

Okay, O. and Sariisik, S. B. (2000). Swelling behavior of poly(acrylamide-co-sodium acrylate) hydrogels in aqueous salt solutions: theory versus experiments. *European Polymer Journal* 36: 393-399.

Ou, Y. X. and Li, J. J. (2006). Flame retardants: properties, preparation and application. *Polymer Degradation and Stability* 91: 2632-2643.

Pascente, J. E. and Pascente T. J. (1998). Method of preventing combustion by applying an aqueous superabsorbent polymer composition. *United States patent*: 5,849,210.

Pourjavadi, A., Harzandi, A.M. and Hosseinzadeh, H. (2004). Modified carrageenan3. Synthesis of a novel polysaccharide-based superabsorbent hydrogel via graft copolymerization of acrylic acid onto kappa carrageenan in air. *European Polymer Journal* 40: 1363–1370.

Rodriguez, R., Alvarez-Lorenzo, C. and Concheiro, A. (2003). Cationic cellulose hydrogels: kinetics of the cross-linking process and characterization as pH-/ion-sensitive drug delivery systems. *Journal Controlled Release* 86: 253–265.

Schartel, B., Bartholmai, M. and Knoll, U. (2006). Some comments on the main fire retardancy mechanisms in polymer nanocomposites. *Polymers for Advanced Technologies* 17: 772–777.

Senkowski, E. B. (1995). Selling a painting program to management. *Journal of Protective Coatings & Linings*: 86-93.

Sinha Ray, S. and Okamoto, M. (2003). Polymer/layered silicate nanocomposites: a review from preparation to processing. *Progress in Polymer Science* 28: 539–1641.

Tang, Q., Wu, J, Sun, H., Fan, S., Hu, D. and Lin, J. (2008). Superabsorbent conducting hydrogel from poly(acrylamide-aniline) with thermo-sensitivity and release properties. *Carbohydrate Polymers* 73: 473–481.

Tjong, S. C. (2006). Synthesis and structure-property characteristics of clay-polymer nanocomposites. *Nanocrystalline Material*s: 311-348.

Travas-Sejdic, J. and Easteal, A. (2000). Study of free-radical copolymerization of acrylamide with 2-acrylamido-2-methyl-1-propane sulphonic acid. *Journal of Applied Polymer Science* 75: 619-628.

Wang, Y. Z. (1997). Flame-retardation design of PET fibers. *Sichuan Science and Technology Press*, Chengdu.

Wang, X. L., Yang, K. K. and Wang, Y. Z. (2001). Physical and chemical effects of diethyl *N*,*N*ʳ-diethanolaminomethylphosphate on flame retardancy of rigid polyurethane foam. *Journal of Applied Polymer Science* 82: 276-282.

Weian, Z., Weib, L. and Yue, F. (2005). Synthesis and properties of a novel hydrogel nanocomposites *Materials Letters* 59: 2876 – 2880.

Wu, W. and Yang, C. Q. (2007). Comparison of different reactive organophosphorus flame retardant agents for cotton. Part II: Fabric flame resistant performance and physical properties. *Polymer Degradation and Stability* 92: 363-369.

Yan, Q., Zhang, W., Lu, G., Su, X. and Ge, C. (2005). Frontal copolymerization synthesis and property characterization of starch-graft-poly(acrylic acid) hydrogels. *Chemical European Journal* 11: 6609–6615.

Yongzhong, J., Shiyang, G., Shuping, X. and Jun, L. (1999). FT-IR spectroscopy of supersaturated aqueous solutions of magnesium borate *Spectrochimica Acta Part A: Molecular and Biomolecular Spectroscopy*, 56: 1291-1297.

Yue, Y., Shen, X. and Wang, P. (2009). Fabrication and characterization of microstructure and pH sensitive interpenetrating networks hydrogel films and application in drug delivery field. *European Polymer Journal* 45: 309–315.

Zeng, Q. H., Yu, A. B., Lu, G. Q. and Paul, D. R. (2005). Clay-based polymer Nanocomposites: Research and commercial development. *Journal of Nanoscience and Nanotechnology* 5: 1574–1592.

Zhang, J., Wang, L. and Wang, A. (2006). Preparation and swelling behavior of fast swelling superabsorbent hydrogels based on starch-g-poly(acrylic acid-co-sodium acrylate). *Macromolecular Materials and Engineering* 29: 612–620.

Zhang, J. and Wang A. (2007). Study on superabsorbent composites. IX : Synthesis, characterization and swelling behaviors of polyacrylamide/clay composites based on various clays. *Reactive & Functional Polymers* 67: 737–745.

Zhang, J, Wang, Q. and Wang, A. (2007). Synthesis and characterization of chitosan-g-poly(acrylic acid)/attapulgite superabsorbent composites. *Carbohydrate Polymers* 68: 367–374.

VITA

Mr. Nattawut Limparyoon was born on January 11, 1984 in Bangkok, Thailand. He graduated with a Bachelor's Degree in Petrochemical and Polymeric materials from the Faculty of Engineer and Industrial Technology, Silpakorn University in 2005. In June 2006, he studied a Masters degree in the Program of Petrochemistry and Polymer Science at the Faculty of Science, Chulalongkorn University and finished the program in 2009.